Supraglacial river forcing of subglacial water storage and diurnal ice sheet motion

Laurence Smith[1], Lauren C Andrews[2], Lincoln H Pitcher[3], Brandon Overstreet[4], Asa Kristina Rennermalm[5], Matthew G Cooper[6], Sarah R. Cooley[7], Jonathan C Ryan[1], Clément Miège[8], Charles Kershner[9], and Claire E. Simpson[10]

[1]Brown University
[2]NASA Goddard Space Flight Center
[3]University of Colorado Boulder
[4]USGS Oregon Water Science Center
[5]Rutgers, The State University of New Jersey
[6]University of California, Los Angeles
[7]WHOI
[8]University of Utah
[9]Reserach Directorate, National Geospatial-Intelligence Agency
[10]RedCastle Resources, Inc.

November 24, 2022

Abstract

Surface melting can alter ice sheet sliding by supplying water to the bed, but subglacial processes driving ice accelerations are complex. We examine linkages between surface runoff, transient subglacial water storage, and short-term ice motion from 168 consecutive hourly measurements of meltwater discharge (i.e. moulin input) and GPS-derived ice surface motion for Rio Behar, a ˜60 km^2 moulin-terminating supraglacial river catchment the southwest Greenland ablation zone. Short-term accelerations in ice speed correlate strongly with lag-corrected measures of surface mass loss, specifically supraglacial river discharge ($r= 0.9$; $p<0.001$). Though our 7-day record cannot address seasonal-scale forcing, diurnal ice accelerations align with normalized differenced supraglacial and proglacial discharge, a proxy for subglacial storage change, better than GPS-derived ice surface uplift. These observations counter theoretical steady-state basal sliding laws and suggest that moulin- and proglacially induced fluctuations in subglacial water storage, rather than absolute subglacial water storage, drive short-term ice accelerations.

Using this Template

Type or paste the appropriate text (title, author list, and corresponding authors) into the template below.

Contents of this document:

- All Supporting text and figures should be included in this document.
- Tables may be included, but can also be uploaded separately, especially if they are larger than one page, or if necessary for retaining table formatting.
- Data sets, large tables, movie files, and audio files should be uploaded separately, following AGU naming conventions. File name and descriptions for these should be included in this template.
- All references should be included in the reference list of the main paper so that they can be indexed, linked, and counted as citations. The reference section does not count toward length limits.

How to fill out this document:

- Insert supporting information content into each appropriate section of the template.
- Figures and tables should appear above each caption.
- To add additional captions, simply copy and paste each sample caption as needed.
- You will be prompted to upload these files on the Upload Files tab during the submission process, using file type "Supporting Information (SI)"

Geophysical Research Letters

Supporting Information for

Supraglacial river forcing of subglacial water storage and diurnal ice sheet motion

L.C. Smith[1,2,3], L.C. Andrews[4], L.H Pitcher[5,3], B.T. Overstreet[6], Å.K. Rennermalm[7], M.G. Cooper[3,8], S.W. Cooley[9,3], J.C. Ryan[1], C. Miège[7,10], C. Kershner[11,13], C.E. Simpson[12,3]

[1]Institute at Brown for Environment and Society (IBES), Brown University, Providence, Rhode Island, 02912, USA

[2]Department of Earth, Environmental, and Planetary Sciences, Brown University, Providence, Rhode Island, 02912, USA

[3]Department of Geography, University of California - Los Angeles, Los Angeles, California, 90095, USA

[4] Global Modeling and Assimilation Office, NASA Goddard Space Flight Center, Greenbelt, Maryland, 20771, USA

[5]Cooperative Institute for Research in Environmental Sciences (CIRES), University of Colorado – Boulder, Boulder, Colorado, 80303, USA

[6]Department of Geology and Geophysics, University of Wyoming, Laramie, WY, 82071, USA

[7]Department of Geography, Rutgers, The State University of New Jersey, New Brunswick, 08901, New Jersey

8Atmospheric Sciences and Global Change Division, Pacific Northwest National Laboratory, Richland, Washington, 99352, USA

[9]Department of Earth System Science, Stanford University, Stanford, CA, 94305Affiliation for author 9.

[10]Department of Geography, University of Utah, Salt Lake City, Utah, 84112, USA

[11]Research Directorate, National Geospatial-Intelligence Agency, Springfield, VA 22150

[12]RedCastle Resources, Inc., Salt Lake City, Utah, 84138, USA

[13]Department of Geography and Geoinformation Science, George Mason University, Fairfax, VA 22030

Contents of this file

Text S1: Supplemental background Text S2: Field collection and data processing of Acoustic Doppler Current Profiler (ADCP) supraglacial river discharge measurements Text S3: Description of variables for full-resolution ADCP datafiles Text S4: Field collection and data processing of GPS ice surface motion measurements Text S5: PROMICE KAN_M Automated Weather Station data and processing Text S6: Proglacial

river discharge data and processing Text S7: Computation of subglacial water storage (S) and subglacial water storage change (ΔS) proxies Text S8: Supplemental discussion of ΔS and ice motion Figure S1: Photograph 1 of ADCP discharge monitoring site Figure S2: Photograph 2 of ADCP discharge monitoring site Figure S3: Photograph 3 of ADCP discharge monitoring site Figure S4: Photograph 4 of ADCP discharge monitoring site Figure S5: Hourly time-series plot of ADCP supraglacial river discharge Figure S6: Photograph of GPS data collection site Figure S7: Correlations between calculated storage proxies and ice motion Table S1: Summary table of hourly ADCP supraglacial river discharge measurements Table S2: Summary table of minimum, maximum and diurnal range of supraglacial river discharge measurements for each calendar day

Additional Supporting Information (Files uploaded separately

Dataset S1: Hourly and daily summary tables of ADCP supraglacial river discharge measurements (Excel format)

Dataset S2: Hourly summary table of ADCP supraglacial river discharge measurements (text format)

Dataset S3: Full-resolution data files for SonTek River Surveyor® M9 Acoustic Doppler Current Profiler (ADCP) transects

Dataset S4: Hourly air temperature, melt energy and ice surface ablation computed from PROMICE KAN_M Automated Weather Station

Dataset S5: GPS-derived ice surface positions and velocity calculations

Δατασετ Σ6: ΓΠΣ-δεριεδ ανδ δισςηαργε-διφφερενςε προξιες φορ συβγλαςιαλ στοραγε (Σ) ανδ συβγλαςιαλ στοραγε ςηανγε (ΔΣ)

Dataset S7: Full-resolution GPS data files of ice surface motion

Dataset S8: Time-lapse camera movie of Rio Behar discharge fluctuations and ADCP data collections

Caption for Dataset S1 Caption for Dataset S2 Caption for Dataset S3 Caption for Dataset S4 Caption for Dataset S5 Caption for Dataset S6

Text S1: Supplemental Background

Each summer, the delivery of supraglacial meltwater to the GrIS bed causes a rapid initial rise in subglacial water pressure, which reduces basal traction and enhances ice sliding (e.g. *Bartholomew et al., 2010, Hoffman et al., 2011; Zwally et al., 2002*). A gradual slowdown in ice motion then occurs as increasing subglacial efficiency reduces regional subglacial pressure and increases basal traction (e.g.,*Bartholomew et al., 2010; Hoffman et al., 2011; 2016*). Superimposed upon this seasonal cycle are short-term accelerations lasting several hours to several days attributed to variations in meltwater input (*Andrews et al., 2014; Schoof, 2010*). In the lower ablation zone, brief increases in ice speed of up to ~300% (with lesser accelerations at higher elevations) are broadly attributed to the effect of diurnal surface melting on subglacial hydrology and water pressure (e.g. *Andrews et al., 2014; Cowton et al., 2016; Davison et al., 2019; Hoffman et al., 2011; Shepherd et al., 2009*).

At a process level, however, the interaction among subglacial cavity evolution, subglacial storage, and ice motion remains difficult to interpret across spatial and temporal scales despite extensive collection of on-ice surface measurements (e.g., *Anderson et al., 2004; Andrews et al., 2018; Bindschadler, 1983; Cowton et al., 2016; Flowers et al., 2016; Hoffman et al., 2011; Howat et al., 2008; Iken et al., 1983; Jansson, 1996; Kamb, 1970; Schweizer & Iken, 1992*). GPS-derived ice surface elevations, in particular, are typically noisy and partitioning the components of uplift is uncertain. This makes interpretation of melt-induced basal uplift and uplift rates in the context of ice motion challenging (e.g. *Andrews et al., 2018, Cowton et al., 2016*). Furthermore, there is a growing appreciation that meltwater surface routing through Greenland's large supraglacial river catchments modulates the magnitude and timing of meltwater runoff entering moulins (*Smith et al. 2017; Yang et al., 2018; 2020*), which must surely influence observed variations in basal water pressure and associated ice velocity (e.g. *Banwell et al. 2016; Clason et al., 2015; Palmer et al., 2011; Pitcher and Smith, 2019; Zwally et al.,2002*). Yet, the influence of supraglacial river discharge on short-term subglacial water storage fluctuations and ice motion has received little observational study.

The purpose of this study is to examine the influence of moulin input (i.e. supraglacial river discharge) on localized, short-term accelerations in ice surface velocity. To achieve this, we explore temporal correlations between hourly time series of surface energy balance, ice ablation, supraglacial river discharge, and horizontal/vertical ice surface motion for Rio Behar, a moderately sized (˜60.2 km^2 in July 2016) mid-elevation (>1200 m a.s.l.) supraglacial river catchment in the southwest Greenland ablation zone (*Smith et al., 2017*). It represents a typical catchment of the snow-free, bare ice ablation zone (*Cooper and Smith, 2019; Ryan et al., 2019*), including intense melting and development of weathering crust development during the month of July (*Cooper et al., 2018*).

The novel datasets analyzed here are: (1) 168 high-quality Acoustic Doppler Current Profiler (ADCP) consecutive hourly measurements of supraglacial river discharge (i.e. catchment runoff flux, m^3 s^{-1}) acquired 6-13 July 2016 approximately 750 m upstream of the Rio Behar terminal moulin; and (2) simultaneous GPS measurements of horizontal and vertical ice surface motion (5-second sampling interval). We also use PROMICE KAN_M AWS data to estimate surface energy inputs and ablation; and compute proxies for subglacial storage (S) and its rate-of-change (ΔS) using both GPS and hydrographic methods. These data are freely available as Additional Supporting Information (**Additional Supporting Information Datasets S1-S7**).

Permanent discharge gauging stations are infeasible in the rapidly melting ablation zone environment. Owing to continuous thermal erosion of the ice bed, empirical stage-discharge rating curves rapidly obsolesce, necessitating that discharges be measured in situ rather than estimated from empirical rating curves relating occasional discharge measurements to continuously recorded water level changes. This requirement of hourly around-the-clock ADCP operations (together with non-trivial logistical challenges of camping and anchoring instruments in rapidly melting bare ice) explain the relative brevity (1 week) of our hourly supraglacial river discharge time series.

Simultaneous measurements of air temperature, radiation, and ice surface ablation were acquired from the nearby PROMICE KAN_M Automated Weather Station (*Fausto and van As, 2019*). Proglacial river discharges from two permanent gauging stations (*Rennermalm et al., 2013b; 2017; van As et al., 2017; 2019*) were also incorporated into this study. The 60.2 km^2 July 2016 Rio Behar catchment boundary was delineated using a fixed-wing drone and WorldView satellite imagery following the methods of *Smith et al. 2017* . This 2016 catchment boundary is presented for illustration purposes in**Figure 1** , but is not otherwise used in this study.

Text S2: Field collection and data processing of Acoustic Doppler Current Profiler (ADCP) supraglacial river discharge measurements

Over the period 5-13 July 2016, a total 847 ADCP transects were acquired at a fixed cross-section (location 67.0499°N, -49. 0180°W) in the main-stem Rio Behar supraglacial river, using field methods based on*Smith et al.* (2017) (**Figures S1-S4**). Of these 847 transects, 677 later passed rigorous quality-assurance screening and were used to compute 174 in situ supraglacial river discharge estimates (**Tables S1-S2; Figure S5**). The 174 measurements were acquired between 13:00:09 UTC on 5 July 2016 and 10:37:57 UTC on 13 July 2016. Of these measurements, 168 were collected consecutively every hour starting 11:34:50 UTC on 6 July 2016 and ending 10:37:57 UTC on 13 July 2016. These 168 consecutive hourly measurements (1 full week) are the moulin input dataset analyzed in this study. The additional 6 discharge measurements collected intermittently on 5/6 July 2013 are excluded from our analysis because they do not fully capture the diurnal cycle, but are included in the archival dataset.

All surveys were conducted using a SonTek River Surveyor® M9 ADCP mounted on a SonTek HydroBoard

II and a moving-boat survey type. To complete each survey, the M9 system was towed, in-transect, back and forth across the Rio Behar Channel, using a custom bank-operated cableway that enabled single-side tensioning and operation (**Figures S1-S4**). Between 3-9 individual hydrographic profiles or transects of channel cross-section, wetted perimeter, and flow velocity were collected during each measurement hour, yielding a total of 847 transects acquired over the field experiment study period (**Tables S1-S2, Additional Supporting Information Datasets S1-S3**)

ADCP data were later processed into high-quality discharge retrievals using the following quality assurance (QA) and quality control (QC) workflow. This QA/QC workflow is similar to that described in*Smith et al.* (2017) and consists of the following:

1. Open all ADCP output files for a given hour in River Surveyor Live (RSL) software and manually check/edit system settings. For all files, the Transducer depth was set to 0.1 m, the magnetic declination was set at -29, GPS reference was set to GGA, and the depth reference was set to Vertical Beam (VB) (rather than Bottom Track, BT).
2. Instrument performance was also validated in RSL. Our system quality checks include: ensuring system power or voltage >9.5, GPS quality >= 3, Horizontal Dilution of Precision (HDOP) <= 2, the track reference was >0. Quality checks were initially conducted manually, and were later automated using Matlab.
3. The edge or bank data for each measurement were manually inspected to confirm that the ADCP was receiving velocity and depth data near the profile edges. Profiles with no edge data (for either or both edges) were discarded from the final hourly discharge estimate.
4. The depth data for each profile were inspected by comparing both the VB and BT data series and determining which depth reference was higher quality (i.e. had fewer outliers and less dropout). If both VB and BT were of equal quality, VB was selected as the depth reference. If VB had substantial dropout or anomalies, BT was selected. If either VB or BT had data dropout whereas the other depth reference contained data, composite tracks were selected such that RSL fills gaps in depth data series. Each profile was manually ranked on a scale from 0 to 3, where 0 or 1 indicates a poor or unusable transect due to insufficient depth data, 2 indicates a profile with minimal outliers and dropout, and 3 indicates a profile with no outliers or dropout. Profiles ranked as 0 or 1 were discarded from the final hourly discharge estimates, unless all transects in a given measurement hour were ranked as 0 or 1. In this instance, all transects were kept unless certain transects had notable more outliers or data dropout than other transects, in which case lower quality transects were removed from the final hourly discharge estimate.
5. Velocity vectors and the signal-to-noise ratio were also inspected manually. Velocity vectors were ranked on a scale of 1 to 3, where 1 indicates minimal perpendicular vectors, substantial drift, or no data, 2 indicates vectors with moderate drift and some vector crossover, and 3 indicates minimal to no drift or crossover. Profiles with a ranking of 1 were discarded from the final hourly discharge estimate.
6. All QA/QC'd data files were exported from River Surveyor Live as Matlab files. Both original ADCP data files (.riv or .rivr) readable in River Surveyor Live (which can be freely downloaded from the SonTek/Xylem website after registering with an email address) and output to Matlab files are available via **Additional Supporting Information Dataset S3** .
7. Following manual/automated QA/QC checks, resultant ADCP data and associated variable descriptions were summarized for each measurement hour. These summary data are presented in **Tables S1-S2** ; and in as **Additional Supporting Information** in Excel spreadsheet (**Dataset S1**) and .txt (**Dataset S2**) formats.

Text S3: Description of variables for full-resolution ADCP datafiles

Sample filename: RioBehar16_adcpQ_hourly_20190731.txt

Variables:

- 'measHr' = measurement hour. Data values range from -6 to 167. We measured discharge (Q) hourly a total of 174 times (of which 168 were continuous hours and analyzed in this study) from 5-13 July 2016, beginning 13:00:09 UTC on 5 July 2016 and ending 10:37:57 UTC on 13 July 2016. The continuous 168 hour record starts at measHr = 0 (11:34:50 UTC on 6 July 2016) with the 6 non-continuous measurements collected prior to measHr = 0 noted as negative measHr values.

- 'startYear' = year at measurement start
- 'startMonth' = month at measurement start
- 'startDay' = day of month at measurement start
- 'startHour' = UTC hour at measurement start
- 'startMinute' = UTC minute at measurement start
- 'startSecond' = UTC second at measurement start
- 'endYear' = year at measurement end
- 'endMonth' = month at measurement end
- 'endDay' = day of month at measurement end
- 'endHour' = UTC hour at measurement end
- 'endMinute' = UTC minute at measurement start
- 'endSecond' = UTC second at measurement start
- 'nFiles' = number of ADCP profiles collected during a measHr
- 'nGood' = number of ADCP profiles flagged as good or usable during QA/QC for a measHr
- 'avgQ' = average of all usable ADCP profiles for a measHr. Units = m^3 s^{-1}'medQ' = median of all usable ADCP profiles for a measHr. Units = m^3s^{-1}
- 'minQ' = minimum of all usable ADCP profiles for a measHr. Units = m^3 s^{-1}
- 'maxQ' = maximum of all usable ADCP profiles for a measHr. Units = m^3 s^{-1}
- 'std' = standard deviation of all usable ADCP profiles for a measHr.
- 'range' = range of all usable ADCP profiles for a measHr. Units = m^3 s^{-1}
- ‘startUtc’ = measurement start date and time in UTC stored as .mat datetime variable
- ‘endUtc’ = measurement end date and time in UTC stored as .mat datetime variable

Text S4: Field collection and data processing of GPS ice surface motion measurements

Records of positional location were collected with a Trimble R7 dual-frequency global positioning system (GPS) receiver and Trimble Zephyr Geodetic antenna (**Figure S6**). The system was installed ˜750 m SSE of the moulin near the ADCP gauging site at location 67.048°N, -49.018 °W, elevation 1211.43 m) The antenna was affixed to a 3.3 m schedule-40 aluminum rod drilled vertically 3 m into the ice. The aluminum rod-antenna setup was allowed to freeze overnight. The system was powered by a 40 W solar panel attached to a weatherproof Pelican hard case that enclosed the GPS receiver, batteries, and cables adjacent to the antenna. The ice sheet thickness at this location is ˜934 m based on Bedmachine v3 (Morlighem et al., 2017). The entire system was provided by UNAVCO (formerly University NAVSTAR Consortium), with protocols for field installation and GPS receiver settings provided by UNAVCO geodetic support engineers. The GPS station recorded positions at 5-s intervals between 5 and 13 July 2016. A base station was also established on bedrock near the ice sheet terminus (67.150°N, 50.058°W, elevation 581.19 m) and recorded positions at 5-s intervals between 4 and 15 July 2016.

Trimble binary receiver files were converted to RINEX observation files using runpkr00 v5.40 and TEQC utilities (*Estey and Meertens* , 1999). On-ice kinematic GPS positions were estimated using carrier-phase differential processing relative to the bedrock mounted reference station (baseline of ˜47 km) using TRACK v1.28 (*Chen* , 1998) and final International GNSS Service satellite orbits following *Andrews et al., 2018; Hoffman et al., 2011* . During processing, kinematic station motion was constrained on an epoch-by-epoch basis to 2,000 m yr^{-1} to permit rapid, short-term velocity changes. The 5-s time series was then smoothed with a 6-hr phase-preserving filter to eliminate spurious signals associated with GPS uncertainties and decimated to a 15-min time series. The smoothed x and y positions were used to calculate 6-hr velocities using a centered time window to limit aliasing that may result from using discrete time intervals. Uncertainties presented here are +/- one standard deviation of the 15-min binned 5-s position data.

Text S5: PROMICE KAN_M Automated Weather Station data and processing

Hourly weather station data were downloaded for the PROMICE KAN_M automated weather station (AWS; *Fausto and van As, 2019* , available at https://www.promice.org/PromiceDataPortal/). The KAN_M AWS is located just outside the 2016 Rio Behar catchment (**Figure 1**). This station, operated by the Geological Survey of Denmark and Greenland, records a range of surface atmospheric variables and ice conditions. Here we use hourly mean energy balance components, surface air temperature and surface ablation measurements to examine the relationship between atmospheric forcing and ice sheet motion. The hourly melt energy (**Figure 2a**) is calculated by summing the net longwave radiation, net shortwave radiation, sensible heat flux and latent heat flux. The shortwave radiation is corrected for any sensor tilt recorded. Sensible heat flux is calculated from the wind speed and temperature gradients between the surface and the sensor height, with an assumed aerodynamic surface roughness of 0.001m. Latent heat flux is calculated from the wind speed and humidity gradients between the surface and sensor height using the same aerodynamic roughness prescribed for sensible heat flux. Air temperature is presented as recorded by the AWS. Ice surface ablation is calculated by differencing the hourly observations of the pressure transducer (drilled into the underlying ice) every 6 hours. During the observation period, the pressure transducer remained fully embedded within the underlying ice and did not need to be reinstalled.

Text S6: Proglacial river discharge data and processing

Hourly proglacial discharges for Qinnguata Kuussua/Watson River (*van As et al., 2017; 2019*) were downloaded from*https://doi.org/10.22008/promice/data/watson_river_discharge*. Proglacial discharges have been recorded at this location since 2006, using in situ pressure transducer measurements of stage (water level) and an empirical stage-discharge rating curve calibrated with intermittent in situ discharge measurements acquired from different techniques including current meters, the float method, and Acoustic Doppler Current Profiler (ADCP) transects. The discharge estimates have an estimated 15% uncertainty due to rating curve fit and errors in cross-sectional area and velocity measurements (*van As et al. 2017*).

Hourly proglacial river discharges in Akuliarusiarsuup Kuua, a major headwater tributary of Qinnguata Kuussua ˜33 km upstream of the Kangerlussuaq bridge and ˜2 km downstream of the ice edge, were downloaded from https://doi.org/10.1594/PANGAEA.876357. Proglacial discharges at Akuliarusiarsuup Kuua have been recorded since 2008 at a road bridge crossing (AK4 station, *Rennermalm et al., 2013b; 2017*). Stage and water temperature data are collected sub-hourly using a Solinst® Levelogger pressure transducer and atmospheric barometric pressure logger (accuracies 0.003 m and 0.05°C for the Levelogger, and 0.001 m for the barologger, respectively). Discharges are estimated from the continuously recorded stage data using an empirical stage-discharge rating curve calibrated by periodic in-situ discharge measurements collected from the bridge, using either USGS-style Price AA current meters or a SonTek River Surveyor® ADCP.

The discharge monitoring station at Kangerlussuaq was chosen as the preferred proglacial discharge dataset due its capture of proglacial outflow from a much larger area of the ice sheet, thus maximizing the likelihood of subglacial linkage to Rio Behar moulin, despite uncertain basal routing in the region (e.g. *Lindbäck et al* ., 2015). To convert the Kangerlussuaq time series into a measure of estimated peak daily discharge at the ice edge, a cross correlation analysis between hourly AK4 and GEUS station measurements was used to determine to estimate the mean timing difference between peak daily flows observed at Kangerlussuaq and peak daily flows at the ice edge.

During the study period, the mean time difference between daily flow peaks at Kangerlussuaq and at AK4 station (33 km distance) averaged 7.6 hours (0.83 s/m). A small additional timing correction between AK4 and the ice edge (2 km distance) is estimated as 0.46 h, by multiplying the mean Kangerlussuaq-AK4 timing correction (0.83 s/m) by 2 km. The total timing correction of 8.1 + 0.9 h was rounded to 8-h and temporally subtracted from daily peak timings observed at Kangerlussuaq bridge. Note that this 8-h proglacial correction is not the same thing as a proglacial flow routing delay because it does not distinguish between wave celerity and Lagrangian flow, but is sufficient for our purpose here, which is simply to estimate the daily timing of peak proglacial outflow at the ice edge using measurements from Kangerlussuaq. Furthermore, note that this

8-h proglacial timing correction does not represent the time difference between peak daily discharge entering Rio Behar moulin and peak daily discharge at the ice edge. Cross-correlation analysis between daily peaks in supraglacial and estimated ice-edge proglacial indicate that the moulin-edge timing difference (again, timing difference only, not subglacial routing) is ˜20-h (Figure 3).

Though we generally use this corrected proglacial discharge during analysis (e.g. Figures 2, 3 & 5), we do remove the immediate linear trend from proglacial discharge when examining the lagged correlation between proglacial discharge and ice speed in order to eliminate the potential for autocorrelation.

Τεξτ Σ7: ὃμπυτατιον οφ συβγλαςιαλ ωατερ στοραγε (Σ) ανδ συβγλαςιαλ ωατερ στοραγε ςηανγε (ΔΣ) προξιες

GPS-derived proxies : GPS-measured vertical ice motion is a combination of three components: the vertical component of mean bed-parallel motion, vertical strain of the ice column, and vertical motion of the ice relative to the bed (due to some combination of cavity formation and till dilation, depending on basal conditions). Ideally, these components may be separated by leveraging local knowledge of ice conditions and, critically, several proximal GPS stations (e.g.,*Anderson et al., 2004; Andrews et al., 2018; Harper et al., 2007; Hoffman et al., 2011; Howat et al., 2008; Mair et al., 2002; Sugiyama & Gudmundsson, 200* 4). In the absence of additional GPS stations, the vertical strain rate cannot be estimated, but during the peak of the melt season changes in vertical strain rates are small and similar to winter background strain rates (e.g., *Andrews et al., 2018*), which are accounted for with a detrending to remove the impact of bed parallel motion (e.g., *Bartholomew et al., 2012; Cowton et al., 2016*).

As such, we detrend the 6-h smoothed z data using the long-term linear trend (**Figure 2c**). This limited correction introduces unquantifiable uncertainties, a particular issue with deriving uplift and basal uplift change from GPS observations. In order to calculate the rate of basal uplift, we calculate the derivative of the detrended elevation data by applying a 6-h differencing of the 15-minute dataset, as done to calculate the horizontal velocity. The detrended elevation and basal uplift rate are considered proxies for subglacial storage (S) and subglacial water storage change (ΔS), respectively (**Figure 2c, Figure 5a**). Our GPS-derived proxy for ΔS , albeit noisy, presents peaks that sometimes align with short-term accelerations in ice speed (**Figure 5a**), unlike our GPS-derived peaks in S (**Figure 2c**).

Discharge-difference proxies: While calculating basal uplift and basal uplift rates from GPS requires either multiple GPS stations or assumptions about vertical strain rate and ice flow orientation, our observations also present opportunity utilize an input-output approach to assess subglacial storage (S) and subglacial water storage change (ΔS) more directly. Input-output methods seek to measure or estimate the discharge of surface meltwater entering a glacier or ice sheet catchment and the discharge of proglacial water release. They have been used on smaller alpine glaciers to capture the role of subglacial water storage and change in water storage in driving short-term ice sheet motion (e.g.*Bartholomaus et al., 2008, 2011*), to compute water balance of a small surface catchment in the Sermeq Avannarleq ablation zone of Greenland (McGrath et al., 2011), and to examine long-term storage in the Russell Glacier using surface mass balance modeling and proglacial discharge measurements (*van As et al., 2017*).

The high-quality supraglacial discharge dataset presented here (**Figure S5, Table S1**) offers a rare in situ “input” suitable for comparison with proglacial output.

However, due to the disparities in the magnitudes of supraglacial and proglacial discharge, we must modify our approach by using the normalized difference between measured supraglacial moulin input and proglacial discharge (**Figure 5b, 5c**). To calculate a qualitative proxy for subglacial storage (S), we calculate the 6h cumulative input and discharge, then normalize both measures of cumulative discharge (e.g. instantaneous input and output) between 0 and 1, then calculate the difference (supraglacial minus proglacial) between these two measurements (**Figure 5b**). Inspection of this Sproxy versus ice speed suggests that local subglacial storage and horizontal ice speed are offset, with ice speed peaking several hours before peak storage; however, once the derivative (ΔS) of the proxy is calculated, the correlation with ice speed improves (Figure 5c; Figure S7). The derivative of the storage calculation is input – output on a 6h interval, which is the same as the

6h position derivative used to calculate smoothed ice speed. The occasional temporal offset between our ΔS proxy and ice speed, as well as a secondary daily peak in both datasets, are discussed next in **SI Text S8** . Note that these discharge-difference calculations represent a fleeting measure of net subglacial water storage (i.e. input minus output), not the time required for subglacial water transport. Therefore, any subglacial routing delays (which are known to range from less than 1 to multiple days in this region, *Chandler et al., 2013; van As et al., 2017*) need not be considered in meltwater S and ΔS proxies.

Τεξτ Σ8: Συππλεμενταλ δισςυσσιον οφ ΔΣ προξψ ανδ ιςε μοτιον

Of the variables examined here, we conclude that supraglacial river discharge is the dominant driver of short-term variations in ice speed at our field site, due to its influence on subglacial water storage change ΔS . In the vicinity of the moulin, ΔS is strongly paced by the integrative nature of upstream surface routing through the Rio Behar catchment, which makes the timing of peak daily moulin input less variable than that of melt energy, air temperature, or ablation (**Figure 3**). Our observed ˜5 h delay between peak melt energy and peak moulin input confirms previous assertions (e.g. *Smith et al., 2017; Yang et al. 2018; 2020*) that surface routing delays through supraglacial stream/river drainage catchments are both non-trivial and predictable and should be explicitly accounted for in studies of short-term ice motion. Unlike melt energy, moulin discharge does not shut down at night (**Figure 4d**), perhaps helping to maintain pressurized water-filled subglacial conduits and resist conduit closure (e.g. as per *Meierbachtol et al., 2013; Bartholomaus et al., 2008*).

Our discharge-difference proxies for S and ΔS rely on a core assumption that proglacial discharges sourced from a large area can reasonably characterize basal water pressure under our much smaller study area; and that supraglacial moulin inputs transfer rapidly to the bed rather than entering englacial storage. Furthermore, we must apply a timing correction to the proglacial discharge record to compensate for the net effects of proglacial flow routing and wave celerity between the ice terminus to Kangerlussuaq bridge (35 km; SI Text S6).

While our supraglacial hydrograph and resultant qualitative ΔSproxy appear to align reasonably well with the ascent of daily peaks in ice speed, we note a varying time lag between ΔS and ice motion, as well as some non-linear behavior on the descending limb of the diurnal peaks (**Figure 5c**). There are a number of possible reasons for these phenomena. One likely reason is that ice motion integrates both local and non-local forcings over long length scales (3-8 ice thicknesses), so ice dynamics from surrounding areas likely influence our field site. Similarly, supraglacial forcing of the subglacial system is not uniform over these length scales, with moulin inputs peaking at different times due to varying upstream catchment areas (*Smith et al., 2017; Yang et al, 2016*). While the Rio Behar moulin has no neighboring large moulins within 5 km, we cannot rule out the possibility of temporally asymmetric subglacial water delivery from nearby moulins. However, we observe a small secondary daily peak in our discharge-difference ΔS proxy that often coincides with a smaller secondary peak or shoulder in daily ice motion (**Figure 5c**) suggesting reasonably good coupling between our regionally-influenced ΔS proxy and local accelerations in ice speed and that this small secondary ice speed peak is driven by subglacial hydrologic dynamics.

Figures and Tables:

Figure S1. Photo 1 of ADCP discharge monitoring site (67.0499°N, -49. 0180°W). A SonTek River Surveyor® M9 Acoustic Doppler Current Profiler (ADCP) mounted on a SonTek HydroBoard II is being ferried across the Rio Behar supraglacial river channel cross-section in southwest Greenland. The ADCP and hydroboard are tethered to a specialized bank-operated cableway developed by the field team for deployment on ice surfaces with wireless (radio frequency) data relay. A total of 847 ADCP profiles were collected 5-13 July, 2016.

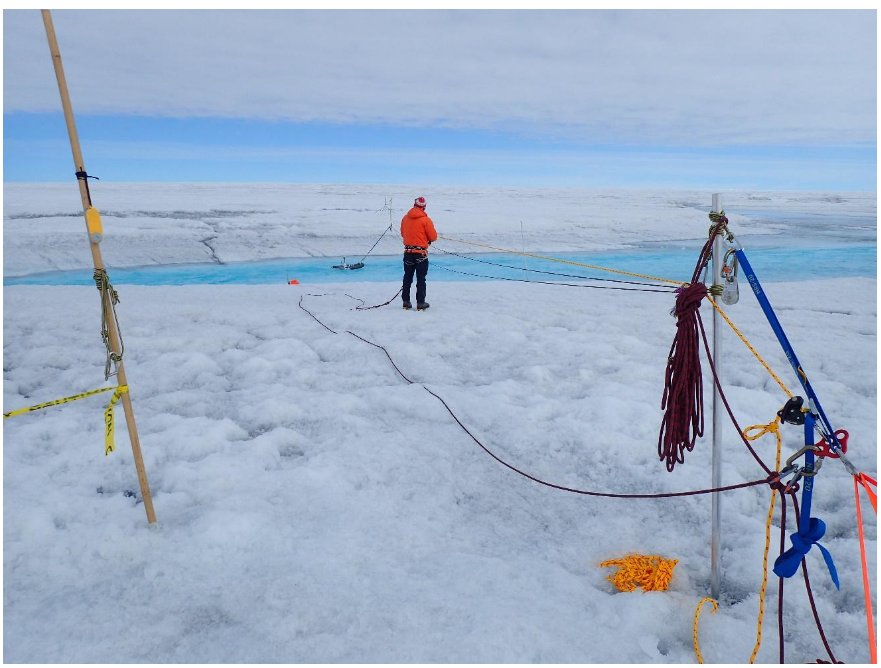

Figure S2. Photo 2 of ADCP discharge monitoring site. The bank-operated cableway requires vertical masts to be drilled into the ice surface on both banks of the river several 10s of m away from the flow. The masts support a tensioned static line and a secondary control line used by roped technicians to safely ferry the ADCP across the channel.

Figure S3. Photo 3 of ADCP discharge monitoring site. Close up photograph of the SonTek River Surveyor® M9 ADCP mounted on a SonTek HydroBoard II.

Figure S4. Photo 4 of ADCP discharge monitoring site. Technicians on the ice bank controlled the ADCP instrument remotely, monitoring its data stream via radio transmissions between the instrument and a laptop computer.

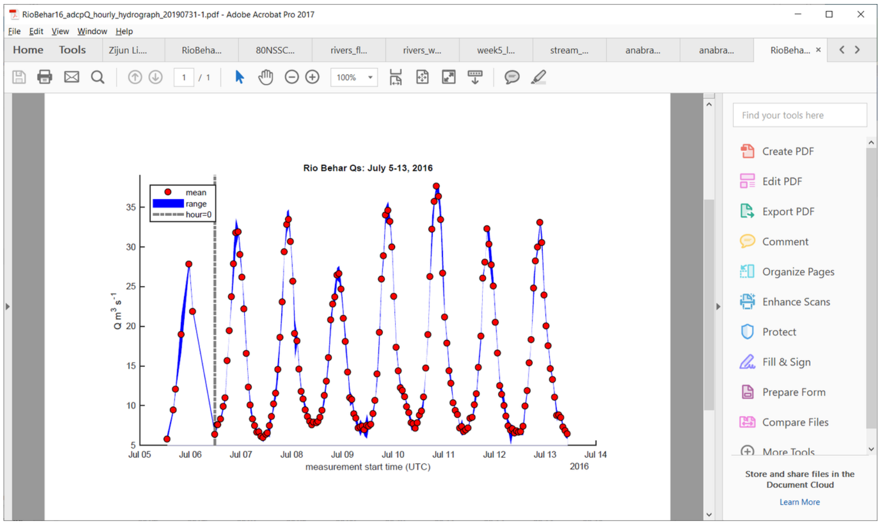

Figure S5. In situ Rio Behar meltwater discharge. Quality-assured ADCP profiles were averaged into a time-series of 174 hourly supraglacial river discharge estimates. A continuous record of 168 consecutive hourly estimates commencing 11:34:50 UTC on 6 July (vertical dashed line) and concluding 10:37:57 UTC on 13 July 2016 forms the basis of this study. Six high-quality discharge measurements acquired July 5-6 were excluded from our analysis due to their intermittency, but are included in archival data.

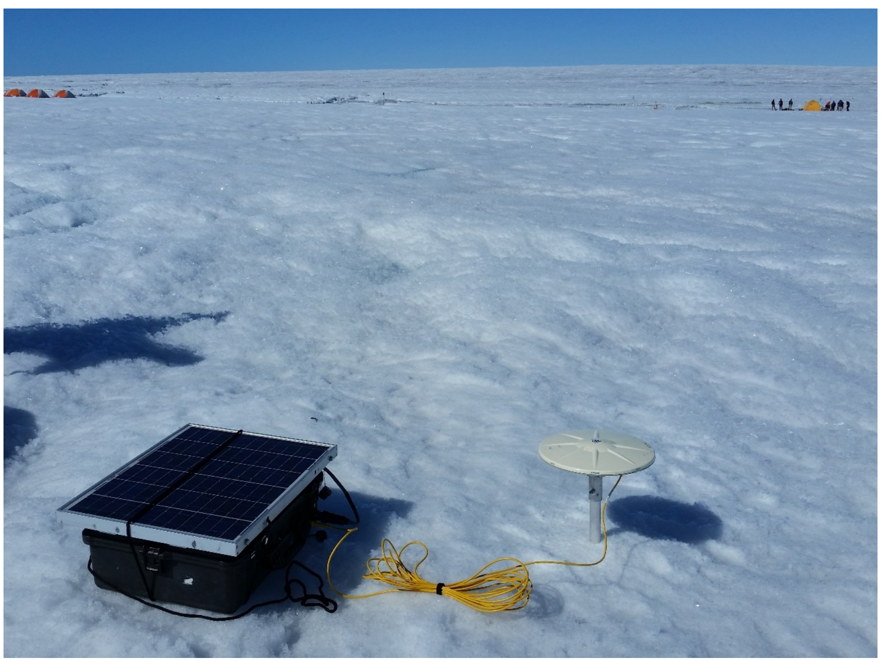

Figure S6 : Photograph of GPS data collection site (67.048°N, -49.018 °W, elevation 1211.43 m). Measurements of ice surface motion were collected every 5 seconds using a Trimble R7 dual-frequency global positioning system (GPS) receiver and Trimble Zephyr GPS antenna affixed to a 3.3 m schedule-40 aluminum pole drilled vertically 3 m into the ice.

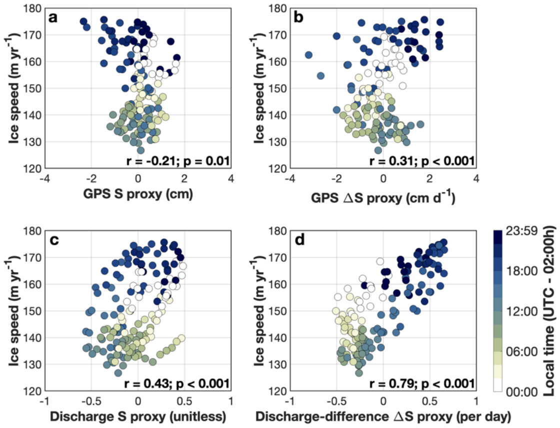

Figure S7. Correlations between calculated subglacial storage proxies and ice motion: (a) GPS-derived storage proxy S (surface elevation), (b) GPS-derived change in storage, ΔS (surface elevation derivative) (c) meltwater-derived storage proxy S (cumulative input- output), and (d) meltwater-derived change in storage, ΔS (6h input-output). These correlations use a cross-correlation value of 0 (e.g. no time offset correction to ice velocity). Linear correlations (r) and p -values indicating statistical significance (p) are shown in the bottom right corner of each plot. Discharge-difference ΔS shows strongest overall correlation with ice speed (r =0.79, panel d).

n	start time (UTC)						end time (UTC)						profiles		Q m³/s	
	yyyy	mm	dd	hr	mi	ss	yyyy	mm	dd	hr	mi	ss	total	good	avg.	std. dev.
-6	2016	7	5	13	0	9	2016	7	5	13	14	34	4	4	5.75	0.45
-5	2016	7	5	15	56	29	2016	7	5	16	3	40	4	4	9.41	0.27
-4	2016	7	5	17	0	5	2016	7	5	17	18	35	7	3	12.03	0.50
-3	2016	7	5	19	40	8	2016	7	5	19	52	46	4	3	18.93	2.34
-2	2016	7	5	23	20	5	2016	7	5	23	29	32	4	4	27.79	0.43
-1	2016	7	6	1	5	14	2016	7	6	1	14	32	4	3	21.82	0.32
0	2016	7	6	11	34	50	2016	7	6	11	43	43	4	3	6.35	0.34
1	2016	7	6	12	40	40	2016	7	6	13	0	45	7	3	7.56	0.38
2	2016	7	6	13	0	56	2016	7	6	13	40	17	7	6	7.56	0.21
3	2016	7	6	14	20	11	2016	7	6	14	31	50	6	4	8.27	0.36
4	2016	7	6	15	35	19	2016	7	6	15	45	52	6	5	9.86	0.29
5	2016	7	6	16	27	52	2016	7	6	16	40	11	6	4	10.95	0.41
6	2016	7	6	17	27	6	2016	7	6	17	35	33	4	2	15.63	0.41
7	2016	7	6	18	27	54	2016	7	6	18	41	54	5	1	19.41	0.00
8	2016	7	6	19	28	56	2016	7	6	19	49	29	7	5	23.68	0.80
9	2016	7	6	20	27	26	2016	7	6	20	37	40	4	4	27.82	1.79
10	2016	7	6	21	30	3	2016	7	6	21	47	40	6	2	31.74	2.62
11	2016	7	6	22	41	2	2016	7	6	22	51	1	4	4	31.85	0.37
12	2016	7	6	23	30	39	2016	7	6	23	50	41	6	5	29.00	0.61
13	2016	7	7	0	26	57	2016	7	7	0	37	14	4	4	26.13	0.14
14	2016	7	7	1	23	38	2016	7	7	1	31	4	4	4	22.14	0.81
15	2016	7	7	2	31	19	2016	7	7	2	40	23	5	3	16.53	0.59
16	2016	7	7	3	30	46	2016	7	7	3	38	10	4	4	12.29	0.33
17	2016	7	7	4	20	48	2016	7	7	4	27	42	4	4	10.03	0.70
18	2016	7	7	5	29	7	2016	7	7	5	35	39	4	4	8.28	0.14
19	2016	7	7	6	27	48	2016	7	7	6	34	14	4	4	7.45	0.53
20	2016	7	7	7	30	36	2016	7	7	7	36	0	4	4	6.61	0.26
21	2016	7	7	8	28	10	2016	7	7	8	37	10	6	5	6.66	0.49
22	2016	7	7	9	28	50	2016	7	7	9	34	8	4	4	6.08	0.24
23	2016	7	7	10	23	47	2016	7	7	10	42	13	9	3	5.93	0.49
24	2016	7	7	11	53	0	2016	7	7	11	58	41	4	4	6.36	0.23
25	2016	7	7	12	31	22	2016	7	7	12	38	49	4	4	6.53	0.33
26	2016	7	7	13	29	25	2016	7	7	13	41	55	6	6	7.44	0.80
27	2016	7	7	14	26	36	2016	7	7	14	34	6	5	3	8.59	0.08
28	2016	7	7	15	27	1	2016	7	7	15	40	53	7	4	10.17	0.57
29	2016	7	7	16	24	58	2016	7	7	16	36	9	6	6	11.53	0.59
30	2016	7	7	17	28	27	2016	7	7	17	42	35	6	5	14.51	1.06
31	2016	7	7	18	29	39	2016	7	7	18	38	42	4	3	18.56	0.54
32	2016	7	7	19	31	53	2016	7	7	19	44	12	6	4	23.02	1.51
33	2016	7	7	20	29	17	2016	7	7	20	41	6	6	2	29.34	0.14
34	2016	7	7	21	40	29	2016	7	7	21	58	33	8	5	32.77	1.01
35	2016	7	7	22	29	45	2016	7	7	22	43	26	4	3	33.42	1.14
36	2016	7	7	23	25	34	2016	7	7	23	34	24	4	4	30.63	0.41
37	2016	7	8	0	33	48	2016	7	8	0	41	25	4	4	25.63	0.58
38	2016	7	8	1	23	55	2016	7	8	1	30	51	4	3	19.04	2.81
39	2016	7	8	2	33	17	2016	7	8	2	40	17	4	4	18.11	0.50
40	2016	7	8	3	27	53	2016	7	8	3	34	42	4	4	14.56	0.40
41	2016	7	8	4	31	11	2016	7	8	4	36	29	4	4	11.75	0.47
42	2016	7	8	5	25	1	2016	7	8	5	31	18	4	4	10.80	0.39
43	2016	7	8	6	26	2	2016	7	8	6	35	4	6	6	9.43	0.52
44	2016	7	8	7	29	10	2016	7	8	7	34	32	4	3	8.59	0.44
45	2016	7	8	8	31	53	2016	7	8	8	36	53	4	4	7.99	0.47
46	2016	7	8	9	31	39	2016	7	8	9	39	25	6	6	7.54	0.33
47	2016	7	8	10	18	9	2016	7	8	10	30	37	6	4	7.89	0.28
48	2016	7	8	11	48	38	2016	7	8	11	59	43	7	6	7.80	0.25
49	2016	7	8	12	30	25	2016	7	8	12	41	38	6	6	7.97	0.22
50	2016	7	8	13	26	25	2016	7	8	13	36	30	6	6	8.50	0.18
51	2016	7	8	14	23	6	2016	7	8	14	30	53	4	4	9.37	0.24
52	2016	7	8	15	29	22	2016	7	8	15	36	16	4	3	11.24	0.80
53	2016	7	8	16	27	52	2016	7	8	16	34	13	4	4	13.04	0.49

Table S1: Hourly ADCP measurements of supraglacial river discharge

n	start time (UTC)						end time (UTC)						profiles		Q m^3/s	
	yyyy	mm	dd	hr	mi	ss	yyyy	mm	dd	hr	mi	ss	total	good	avg.	std. dev.
-6	2016	7	5	13	0	9	2016	7	5	13	14	34	4	4	5.75	0.45
-5	2016	7	5	15	56	29	2016	7	5	16	3	40	4	4	9.41	0.27
-4	2016	7	5	17	0	5	2016	7	5	17	18	35	7	3	12.03	0.50
-3	2016	7	5	19	40	8	2016	7	5	19	52	46	4	3	18.93	2.34
-2	2016	7	5	23	20	5	2016	7	5	23	29	32	4	4	27.79	0.43
-1	2016	7	6	1	5	14	2016	7	6	1	14	32	4	3	21.82	0.32
0	2016	7	6	11	34	50	2016	7	6	11	43	43	4	3	6.35	0.34
1	2016	7	6	12	40	40	2016	7	6	13	0	45	7	3	7.56	0.38
2	2016	7	6	13	0	56	2016	7	6	13	40	17	7	6	7.56	0.21
3	2016	7	6	14	20	11	2016	7	6	14	31	50	6	4	8.27	0.36
4	2016	7	6	15	35	19	2016	7	6	15	45	52	6	5	9.86	0.29
5	2016	7	6	16	27	52	2016	7	6	16	40	11	6	4	10.95	0.41
6	2016	7	6	17	27	6	2016	7	6	17	35	33	4	2	15.63	0.41
7	2016	7	6	18	27	54	2016	7	6	18	41	54	5	1	19.41	0.00
8	2016	7	6	19	28	56	2016	7	6	19	49	29	7	5	23.68	0.80
9	2016	7	6	20	27	26	2016	7	6	20	37	40	4	4	27.82	1.79
10	2016	7	6	21	30	3	2016	7	6	21	47	40	6	2	31.74	2.62
11	2016	7	6	22	41	2	2016	7	6	22	51	1	4	4	31.85	0.37
12	2016	7	6	23	30	39	2016	7	6	23	50	41	6	5	29.00	0.61
13	2016	7	7	0	26	57	2016	7	7	0	37	14	4	4	26.13	0.14
14	2016	7	7	1	23	38	2016	7	7	1	31	4	4	4	22.14	0.81
15	2016	7	7	2	31	19	2016	7	7	2	40	23	5	3	16.53	0.59
16	2016	7	7	3	30	46	2016	7	7	3	38	10	4	4	12.29	0.33
17	2016	7	7	4	20	48	2016	7	7	4	27	42	4	4	10.03	0.70
18	2016	7	7	5	29	7	2016	7	7	5	35	39	4	4	8.28	0.14
19	2016	7	7	6	27	48	2016	7	7	6	34	14	4	4	7.45	0.53
20	2016	7	7	7	30	36	2016	7	7	7	36	0	4	4	6.61	0.26
21	2016	7	7	8	28	10	2016	7	7	8	37	10	6	5	6.66	0.49
22	2016	7	7	9	28	50	2016	7	7	9	34	8	4	4	6.08	0.24
23	2016	7	7	10	23	47	2016	7	7	10	42	13	9	3	5.93	0.49
24	2016	7	7	11	53	0	2016	7	7	11	58	41	4	4	6.36	0.23
25	2016	7	7	12	31	22	2016	7	7	12	38	49	4	4	6.53	0.33
26	2016	7	7	13	29	25	2016	7	7	13	41	55	6	6	7.44	0.80
27	2016	7	7	14	26	36	2016	7	7	14	34	6	5	3	8.59	0.08
28	2016	7	7	15	27	1	2016	7	7	15	40	53	7	4	10.17	0.57
29	2016	7	7	16	24	58	2016	7	7	16	36	9	6	6	11.53	0.59
30	2016	7	7	17	28	27	2016	7	7	17	42	35	6	5	14.51	1.06
31	2016	7	7	18	29	39	2016	7	7	18	38	42	4	3	18.56	0.54
32	2016	7	7	19	31	53	2016	7	7	19	44	12	6	4	23.02	1.51
33	2016	7	7	20	29	17	2016	7	7	20	41	6	6	2	29.34	0.14
34	2016	7	7	21	40	29	2016	7	7	21	58	33	8	5	32.77	1.01
35	2016	7	7	22	29	45	2016	7	7	22	43	26	4	3	33.42	1.14
36	2016	7	7	23	25	34	2016	7	7	23	34	24	4	4	30.63	0.41
37	2016	7	8	0	33	48	2016	7	8	0	41	25	4	4	25.63	0.58
38	2016	7	8	1	23	55	2016	7	8	1	30	51	4	3	19.04	2.81
39	2016	7	8	2	33	17	2016	7	8	2	40	17	4	4	18.11	0.50
40	2016	7	8	3	27	53	2016	7	8	3	34	42	4	4	14.56	0.40
41	2016	7	8	4	31	11	2016	7	8	4	36	29	4	4	11.75	0.47
42	2016	7	8	5	25	1	2016	7	8	5	31	18	4	4	10.80	0.39
43	2016	7	8	6	26	2	2016	7	8	6	35	4	6	6	9.43	0.52
44	2016	7	8	7	29	10	2016	7	8	7	34	32	4	3	8.59	0.44
45	2016	7	8	8	31	53	2016	7	8	8	36	53	4	4	7.99	0.47
46	2016	7	8	9	31	39	2016	7	8	9	39	25	6	6	7.54	0.33
47	2016	7	8	10	18	9	2016	7	8	10	30	37	6	4	7.89	0.28
48	2016	7	8	11	48	38	2016	7	8	11	59	43	7	6	7.80	0.25
49	2016	7	8	12	30	25	2016	7	8	12	41	38	6	6	7.97	0.22
50	2016	7	8	13	26	25	2016	7	8	13	36	30	6	6	8.50	0.18
51	2016	7	8	14	23	6	2016	7	8	14	30	53	4	4	9.37	0.24
52	2016	7	8	15	29	22	2016	7	8	15	36	16	4	3	11.24	0.80
53	2016	7	8	16	27	52	2016	7	8	16	34	13	4	4	13.04	0.49

n	start time (UTC)						end time (UTC)						profiles		Q m^3/s	
	yyyy	mm	dd	hr	mi	ss	yyyy	mm	dd	hr	mi	ss	total	good	avg.	std. dev.
-6	2016	7	5	13	0	9	2016	7	5	13	14	34	4	4	5.75	0.45
-5	2016	7	5	15	56	29	2016	7	5	16	3	40	4	4	9.41	0.27
-4	2016	7	5	17	0	5	2016	7	5	17	18	35	7	3	12.03	0.50
-3	2016	7	5	19	40	8	2016	7	5	19	52	46	4	3	18.93	2.34
-2	2016	7	5	23	20	5	2016	7	5	23	29	32	4	4	27.79	0.43
-1	2016	7	6	1	5	14	2016	7	6	1	14	32	4	3	21.82	0.32
0	2016	7	6	11	34	50	2016	7	6	11	43	43	4	3	6.35	0.34
1	2016	7	6	12	40	40	2016	7	6	13	0	45	7	3	7.56	0.38
2	2016	7	6	13	0	56	2016	7	6	13	40	17	7	6	7.56	0.21
3	2016	7	6	14	20	11	2016	7	6	14	31	50	6	4	8.27	0.36
4	2016	7	6	15	35	19	2016	7	6	15	45	52	6	5	9.86	0.29
5	2016	7	6	16	27	52	2016	7	6	16	40	11	6	4	10.95	0.41
6	2016	7	6	17	27	6	2016	7	6	17	35	33	4	2	15.63	0.41
7	2016	7	6	18	27	54	2016	7	6	18	41	54	5	1	19.41	0.00
8	2016	7	6	19	28	56	2016	7	6	19	49	29	7	5	23.68	0.80
9	2016	7	6	20	27	26	2016	7	6	20	37	40	4	4	27.82	1.79
10	2016	7	6	21	30	3	2016	7	6	21	47	40	6	2	31.74	2.62
11	2016	7	6	22	41	2	2016	7	6	22	51	1	4	4	31.85	0.37
12	2016	7	6	23	30	39	2016	7	6	23	50	41	6	5	29.00	0.61
13	2016	7	7	0	26	57	2016	7	7	0	37	14	4	4	26.13	0.14
14	2016	7	7	1	23	38	2016	7	7	1	31	4	4	4	22.14	0.81
15	2016	7	7	2	31	19	2016	7	7	2	40	23	5	3	16.53	0.59
16	2016	7	7	3	30	46	2016	7	7	3	38	10	4	4	12.29	0.33
17	2016	7	7	4	20	48	2016	7	7	4	27	42	4	4	10.03	0.70
18	2016	7	7	5	29	7	2016	7	7	5	35	39	4	4	8.28	0.14
19	2016	7	7	6	27	48	2016	7	7	6	34	14	4	4	7.45	0.53
20	2016	7	7	7	30	36	2016	7	7	7	36	0	4	4	6.61	0.26
21	2016	7	7	8	28	10	2016	7	7	8	37	10	6	5	6.66	0.49
22	2016	7	7	9	28	50	2016	7	7	9	34	8	4	4	6.08	0.24
23	2016	7	7	10	23	47	2016	7	7	10	42	13	9	3	5.93	0.49
24	2016	7	7	11	53	0	2016	7	7	11	58	41	4	4	6.36	0.23
25	2016	7	7	12	31	22	2016	7	7	12	38	49	4	4	6.53	0.33
26	2016	7	7	13	29	25	2016	7	7	13	41	55	6	6	7.44	0.80
27	2016	7	7	14	26	36	2016	7	7	14	34	6	5	3	8.59	0.08
28	2016	7	7	15	27	1	2016	7	7	15	40	53	7	4	10.17	0.57
29	2016	7	7	16	24	58	2016	7	7	16	36	9	6	6	11.53	0.59
30	2016	7	7	17	28	27	2016	7	7	17	42	35	6	5	14.51	1.06
31	2016	7	7	18	29	39	2016	7	7	18	38	42	4	3	18.56	0.54
32	2016	7	7	19	31	53	2016	7	7	19	44	12	6	4	23.02	1.51
33	2016	7	7	20	29	17	2016	7	7	20	41	6	6	2	29.34	0.14
34	2016	7	7	21	40	29	2016	7	7	21	58	33	8	5	32.77	1.01
35	2016	7	7	22	29	45	2016	7	7	22	43	26	4	3	33.42	1.14
36	2016	7	7	23	25	34	2016	7	7	23	34	24	4	4	30.63	0.41
37	2016	7	8	0	33	48	2016	7	8	0	41	25	4	4	25.63	0.58
38	2016	7	8	1	23	55	2016	7	8	1	30	51	4	3	19.04	2.81
39	2016	7	8	2	33	17	2016	7	8	2	40	17	4	4	18.11	0.50
40	2016	7	8	3	27	53	2016	7	8	3	34	42	4	4	14.56	0.40
41	2016	7	8	4	31	11	2016	7	8	4	36	29	4	4	11.75	0.47
42	2016	7	8	5	25	1	2016	7	8	5	31	18	4	4	10.80	0.39
43	2016	7	8	6	26	2	2016	7	8	6	35	4	6	6	9.43	0.52
44	2016	7	8	7	29	10	2016	7	8	7	34	32	4	3	8.59	0.44
45	2016	7	8	8	31	53	2016	7	8	8	36	53	4	4	7.99	0.47
46	2016	7	8	9	31	39	2016	7	8	9	39	25	6	6	7.54	0.33
47	2016	7	8	10	18	9	2016	7	8	10	30	37	6	4	7.89	0.28
48	2016	7	8	11	48	38	2016	7	8	11	59	43	7	6	7.80	0.25
49	2016	7	8	12	30	25	2016	7	8	12	41	38	6	6	7.97	0.22
50	2016	7	8	13	26	25	2016	7	8	13	36	30	6	6	8.50	0.18
51	2016	7	8	14	23	6	2016	7	8	14	30	53	4	4	9.37	0.24
52	2016	7	8	15	29	22	2016	7	8	15	36	16	4	3	11.24	0.80
53	2016	7	8	16	27	52	2016	7	8	16	34	13	4	4	13.04	0.49

n	start time (UTC)						end time (UTC)						profiles		Q m^3/s	
	yyyy	mm	dd	hr	mi	ss	yyyy	mm	dd	hr	mi	ss	total	good	avg.	std. dev.
-6	2016	7	5	13	0	9	2016	7	5	13	14	34	4	4	5.75	0.45
-5	2016	7	5	15	56	29	2016	7	5	16	3	40	4	4	9.41	0.27
-4	2016	7	5	17	0	5	2016	7	5	17	18	35	7	3	12.03	0.50
-3	2016	7	5	19	40	8	2016	7	5	19	52	46	4	3	18.93	2.34
-2	2016	7	5	23	20	5	2016	7	5	23	29	32	4	4	27.79	0.43
-1	2016	7	6	1	5	14	2016	7	6	1	14	32	4	3	21.82	0.32
0	2016	7	6	11	34	50	2016	7	6	11	43	43	4	3	6.35	0.34
1	2016	7	6	12	40	40	2016	7	6	13	0	45	7	3	7.56	0.38
2	2016	7	6	13	0	56	2016	7	6	13	40	17	7	6	7.56	0.21
3	2016	7	6	14	20	11	2016	7	6	14	31	50	6	4	8.27	0.36
4	2016	7	6	15	35	19	2016	7	6	15	45	52	6	5	9.86	0.29
5	2016	7	6	16	27	52	2016	7	6	16	40	11	6	4	10.95	0.41
6	2016	7	6	17	27	6	2016	7	6	17	35	33	4	2	15.63	0.41
7	2016	7	6	18	27	54	2016	7	6	18	41	54	5	1	19.41	0.00
8	2016	7	6	19	28	56	2016	7	6	19	49	29	7	5	23.68	0.80
9	2016	7	6	20	27	26	2016	7	6	20	37	40	4	4	27.82	1.79
10	2016	7	6	21	30	3	2016	7	6	21	47	40	6	2	31.74	2.62
11	2016	7	6	22	41	2	2016	7	6	22	51	1	4	4	31.85	0.37
12	2016	7	6	23	30	39	2016	7	6	23	50	41	6	5	29.00	0.61
13	2016	7	7	0	26	57	2016	7	7	0	37	14	4	4	26.13	0.14
14	2016	7	7	1	23	38	2016	7	7	1	31	4	4	4	22.14	0.81
15	2016	7	7	2	31	19	2016	7	7	2	40	23	5	3	16.53	0.59
16	2016	7	7	3	30	46	2016	7	7	3	38	10	4	4	12.29	0.33
17	2016	7	7	4	20	48	2016	7	7	4	27	42	4	4	10.03	0.70
18	2016	7	7	5	29	7	2016	7	7	5	35	39	4	4	8.28	0.14
19	2016	7	7	6	27	48	2016	7	7	6	34	14	4	4	7.45	0.53
20	2016	7	7	7	30	36	2016	7	7	7	36	0	4	4	6.61	0.26
21	2016	7	7	8	28	10	2016	7	7	8	37	10	6	5	6.66	0.49
22	2016	7	7	9	28	50	2016	7	7	9	34	8	4	4	6.08	0.24
23	2016	7	7	10	23	47	2016	7	7	10	42	13	9	3	5.93	0.49
24	2016	7	7	11	53	0	2016	7	7	11	58	41	4	4	6.36	0.23
25	2016	7	7	12	31	22	2016	7	7	12	38	49	4	4	6.53	0.33
26	2016	7	7	13	29	25	2016	7	7	13	41	55	6	6	7.44	0.80
27	2016	7	7	14	26	36	2016	7	7	14	34	6	5	3	8.59	0.08
28	2016	7	7	15	27	1	2016	7	7	15	40	53	7	4	10.17	0.57
29	2016	7	7	16	24	58	2016	7	7	16	36	9	6	6	11.53	0.59
30	2016	7	7	17	28	27	2016	7	7	17	42	35	6	5	14.51	1.06
31	2016	7	7	18	29	39	2016	7	7	18	38	42	4	3	18.56	0.54
32	2016	7	7	19	31	53	2016	7	7	19	44	12	6	4	23.02	1.51
33	2016	7	7	20	29	17	2016	7	7	20	41	6	6	2	29.34	0.14
34	2016	7	7	21	40	29	2016	7	7	21	58	33	8	5	32.77	1.01
35	2016	7	7	22	29	45	2016	7	7	22	43	26	4	3	33.42	1.14
36	2016	7	7	23	25	34	2016	7	7	23	34	24	4	4	30.63	0.41
37	2016	7	8	0	33	48	2016	7	8	0	41	25	4	4	25.63	0.58
38	2016	7	8	1	23	55	2016	7	8	1	30	51	4	3	19.04	2.81
39	2016	7	8	2	33	17	2016	7	8	2	40	17	4	4	18.11	0.50
40	2016	7	8	3	27	53	2016	7	8	3	34	42	4	4	14.56	0.40
41	2016	7	8	4	31	11	2016	7	8	4	36	29	4	4	11.75	0.47
42	2016	7	8	5	25	1	2016	7	8	5	31	18	4	4	10.80	0.39
43	2016	7	8	6	26	2	2016	7	8	6	35	4	6	6	9.43	0.52
44	2016	7	8	7	29	10	2016	7	8	7	34	32	4	3	8.59	0.44
45	2016	7	8	8	31	53	2016	7	8	8	36	53	4	4	7.99	0.47
46	2016	7	8	9	31	39	2016	7	8	9	39	25	6	6	7.54	0.33
47	2016	7	8	10	18	9	2016	7	8	10	30	37	6	4	7.89	0.28
48	2016	7	8	11	48	38	2016	7	8	11	59	43	7	6	7.80	0.25
49	2016	7	8	12	30	25	2016	7	8	12	41	38	6	6	7.97	0.22
50	2016	7	8	13	26	25	2016	7	8	13	36	30	6	6	8.50	0.18
51	2016	7	8	14	23	6	2016	7	8	14	30	53	4	4	9.37	0.24
52	2016	7	8	15	29	22	2016	7	8	15	36	16	4	3	11.24	0.80
53	2016	7	8	16	27	52	2016	7	8	16	34	13	4	4	13.04	0.49

Table S2. Minimum, maximum and diurnal range of our ADCP supraglacial river discharge measurements for each calendar day

Dataset Captions:

Data Set S1. Summary data tables for hourly Acoustic Doppler Current Profiler (ADCP) supraglacial river discharge measurements, acquired 5-13 July 2017 (Excel spreadsheet format)

Data Set S2. Summary data for hourly Acoustic Doppler Current Profiler (ADCP) supraglacial river discharge measurements, acquired 5-13 July 2017 (Plain Text format)

Data Set S3. Full-resolution cross-sectional Acoustic Doppler Current Profiler (ADCP) data files for SonTek River Surveyor® M9 transects, acquired 5-13 July 2017

Data Set S4 . Hourly air temperature, melt energy and ice surface ablation time series computed from PROMICE KAN-M Automated Weather Station measurements, July 2016

Data Set S5. GPS-derived ice surface positions, uncertainties, and 6h ice speed calculations, acquired 5-14 July 2016.

Data Set S6. Hourly GPS-derived and discharge-difference proxies for subglacial storage (S) and subglacial storage change (ΔS), including uncertainties, calculated for 6-13 July 2016.

Data Set S7. Full-resolution GPS datafiles of ice surface motion

Data Set S8. Time-lapse camera movie of Rio Behar water level fluctuations and ADCP data collections at our discharge monitoring site.

` `

Supraglacial river forcing of subglacial water storage and diurnal ice sheet motion

L.C. Smith[1,2,3], L.C. Andrews[4], L.H Pitcher[5,3], B.T. Overstreet[6], Å.K. Rennermalm[7], M.G. Cooper[3,8], S.W. Cooley[9,3], J.C. Ryan[1], C. Miège[7,10], C. Kershner[11,13], C.E. Simpson[12,3]

[1]Institute at Brown for Environment and Society (IBES), Brown University, Providence, Rhode Island, 02912, USA

[2]Department of Earth, Environmental, and Planetary Sciences, Brown University, Providence, Rhode Island, 02912, USA

[3]Department of Geography, University of California - Los Angeles, Los Angeles, California, 90095, USA

[4] Global Modeling and Assimilation Office, NASA Goddard Space Flight Center, Greenbelt, Maryland, 20771, USA

[5]Cooperative Institute for Research in Environmental Sciences (CIRES), University of Colorado – Boulder, Boulder, Colorado, 80303, USA

[6]Department of Geology and Geophysics, University of Wyoming, Laramie, WY, 82071, USA

[7]Department of Geography, Rutgers, The State University of New Jersey, New Brunswick, 08901, New Jersey

8Atmospheric Sciences and Global Change Division, Pacific Northwest National Laboratory, Richland, Washington, 99352, USA

[9]Department of Earth System Science, Stanford University, Stanford, CA, 94305Affiliation for author 9.

[10]Department of Geography, University of Utah, Salt Lake City, Utah, 84112, USA

[11]Research Directorate, National Geospatial-Intelligence Agency, Springfield, VA 22150

[12]RedCastle Resources, Inc., Salt Lake City, Utah, 84138, USA

[13]Department of Geography and Geoinformation Science, George Mason University, Fairfax, VA 22030

Corresponding author: first and last name (laurence_smith@brown.edu)

Key Points:

- We present coincident field measurements of supraglacial river discharge and GPS-derived ice motion on the southwest Greenland Ice Sheet ablation zone
- The measurements are obtained upstream of a major moulin, enabling study of how supraglacial meltwater runoff influences subglacial hydrology and ice motion
- Recorded ice velocities are strongly correlated with measurements of supraglacial river discharge acquired hourly over the 7-day study period
- Differencing of supra- and proglacial discharge hydrographs suggests that diurnal fluctuations in subglacial water storage drive short-term variations in ice motion

Abstract (150 words max)

Surface melting can alter ice sheet sliding by supplying water to the bed, but subglacial processes driving ice accelerations are complex. We examine linkages between surface runoff, transient subglacial water storage, and short-term ice motion from 168 consecutive hourly measurements of meltwater discharge (i.e. moulin input) and GPS-derived ice surface motion for Rio Behar, a ~60 km^2 moulin-terminating supraglacial river catchment the southwest Greenland ablation zone. Short-term accelerations in ice speed correlate strongly with lag-corrected measures of surface mass loss, specifically supraglacial river discharge ($r= 0.9$; $p<0.001$). Though our 7-day record cannot address seasonal-scale forcing, diurnal ice accelerations align with normalized differenced supraglacial and proglacial discharge, a proxy for subglacial storage change, better than GPS-derived ice surface uplift. These observations counter theoretical steady-state basal sliding laws and suggest that moulin- and proglacially induced fluctuations in subglacial water storage, rather than absolute subglacial water storage, drive short-term ice accelerations.

Plain Language Summary

The importance of surface melting to Greenland ice sheet subglacial hydrology and ice sliding dynamics is widely recognized but poorly constrained by field observations. We present 168 consecutive hours of rare in-situ meltwater runoff measurements from a large supraglacial river draining the ice sheet surface, just upstream of its plummet into a major moulin. GPS measurements of ice surface motion record brief accelerations in ice sliding speed that follow daily cycles in meltwater entering the moulin. By comparing these measurements with proglacial river discharges leaving the ice sheet, we identify daily fluctuations in subglacial water storage that align with short-term accelerations in ice motion. These findings affirm the importance of supraglacial rivers to subglacial water pressure and ice dynamics, even in relatively thick ice >40 km inland from the ice terminus.

1. Introduction

Accurate models of ice-sheet response to climate change require good physical understanding of interactions between surface melting, subglacial hydrology, and ice dynamics (e.g., *Bell, 2008; Chu, 2014; Davison et al., 2019*). On the Greenland Ice Sheet (GrIS) ablation zone, surface melting activates a perennial hydrologic system of supraglacial streams, rivers, and lakes (*Irvine-Fynn et al., 2011; Rennermalm et al., 2013a; Lampkin and VanderBerg, 2014; Pitcher and Smith, 2019*), which commonly drain into moulins forming a dynamic subglacial drainage system that modifies basal pressures and ice motion (*e.g. Meierbachtol et al., 2013; Van de Wal et al., 2008; Zwally et al., 2002; Bartholomew et al., 2012*). While early concerns about warming-induced runaway sliding now seem unfounded (e.g. *Tedstone, et al., 2013; 2015; van de Wal et al., 2015; Flowers, 2018*), physical processes governing the link between GrIS supraglacial meltwater runoff, ice sheet basal pressures, and ice sliding remain under intense study (*Davison et al., 2019; Nienow et al., 2017; Williams et al. 2020*).

Traditional basal sliding law formulations linking subglacial pressure and ice motion assume steady-state cavities at the bed (e.g. *Bindschadler, 1983; Schoof, 2005; Gagliardini et al., 2007*). However, observational research suggests that subglacial cavities constantly undergo transient evolution in response to fluctuations in supraglacial meltwater supply and subglacial channelization (*Iken et al., 1983; Bartholomaus et al., 2008; Hoffman et al., 2011; Cowton et al., 2016; Andrews et al., 2018*). If so, highest subglacial water pressures (and therefore ice sliding speed) should occur when transient cavities are growing fastest, not when they are largest (*Iken et al., 1983; Cowton et al., 2016*).

Evidence for transient cavity evolution is drawn primarily from GPS-derived correlations of horizontal ice speed with vertical ice surface uplift (interpreted as a proxy for total subglacial water storage, *S*) or its first derivative (interpreted as subglacial water storage rate-of-change, ΔS). GrIS horizontal ice sliding speed broadly covaries with vertical surface uplift over the time scale of a melt season (e.g., *Hoffman et al., 2011; Bartholomew et al., 2010; Bartholomew et al., 2012*), but variations at shorter timescales tend to correlate better with its derivative (*Hoffman et al., 2011; Cowton et al., 2016; Andrews et al., 2018*). Such correlations are typically weak and spatially variable due to a range of confounding factors impeding calculation of basal uplift from ice surface elevation measurements (see *Andrews et al., 2018* and *Hoffman et al., 2011*). Therefore, it is difficult to infer interactions between surface melting, subglacial water storage, cavity growth, and ice motion for the GrIS, despite previous success on alpine glaciers (e.g. *Bartholomaus et al., 2008; 2011*).

To study the links among supraglacial runoff, subglacial water storage fluctuations, and short-term ice motion, we present in situ measurements of moulin input (i.e. supraglacial discharge), ice surface speed, and ice surface uplift for Rio Behar, a large supraglacial river on the GrIS mid-elevation (>1200 m a.s.l.) ablation zone (**Figure 1**). We compare daily cycles in these variables with PROMICE automated weather station measurements of surface energy balance and ablation (*Fausto and van As, 2019*), and with proglacial discharges from permanent river gauging stations located downstream (*Rennermalm et al., 2013b; 2017; van As et al., 2018; 2019*). Horizontal GPS positions provide ice surface speed variations, and vertical GPS positions and their first derivative provide proxies for subglacial storage *S* and rate-of-change ΔS, respectively. We also compute alternate, qualitative proxies for *S* and ΔS by differencing normalized supraglacial and proglacial discharge hydrographs (adapted from *Bartholomaus et al., 2008, 2011* and *McGrath et al., 2011*). We conclude that diurnal cycles in moulin input influence local ice speed variations through their influence on Δ*S*, confirming that transient water storage and cavity growth are important drivers of subglacial basal pressure and short-term ice motion.

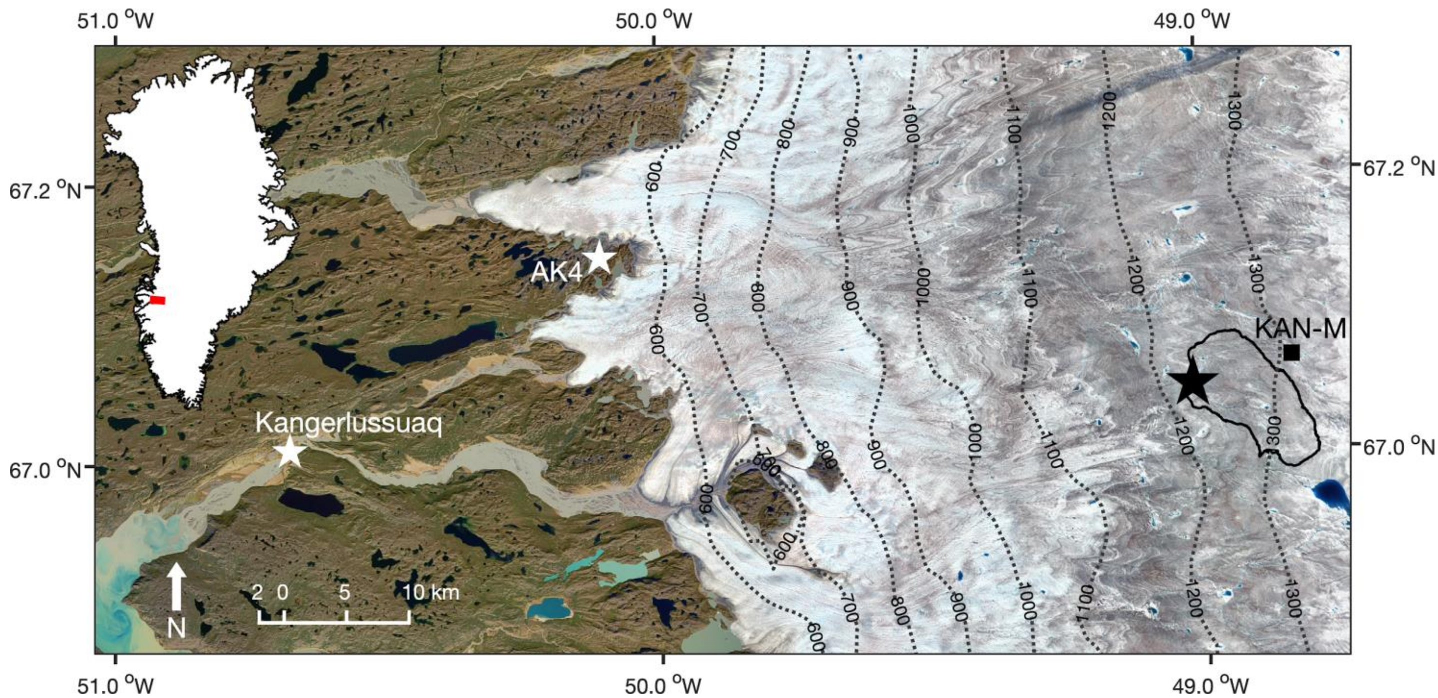

Figure 1: Study area in southwest Greenland. Black star shows location of our GPS measurements of ice surface motion and Acoustic Doppler Current Profiler (ADCP) measurements of moulin input (supraglacial discharge) in Rio Behar, a large supraglacial river penetrating the ice sheet >40 km from the ice edge. Measurements were acquired ~750 m upstream of the Rio Behar terminal moulin from 5-14 July 2017. Black outline denotes the Rio Behar surface catchment (60.02 km² in July 2016). White stars show locations of the PROMICE KAN_M automated weather station (black square) and two permanent gauging stations in proglacial rivers. Background is a 26 July 2016 true-color Landsat-8 satellite image.

2. Data and Methods

2.1 Observational data

In July 2016 the Rio Behar terminal moulin was located at 67.047°N, -49.033°W, with an upstream drainage catchment of ~60.2 km^2 and mean surface elevation >1200 m (**Figure 1**). We established a field camp to monitor moulin meltwater input ~750 m upstream (location ~67.0499°N, -49. 0180°W) and ice surface motion. Field operations were carried out from 5-14 July 2016, with 168 consecutive hourly measurements of supraglacial river discharge collected 6-13 July using a SonTek RiverSurveyor M9 Acoustic Doppler Current Profiler (ADCP) and methods of *Smith et al. (2017)*. A Tyrolean cableway was suspended over the river to safely and repeatedly tow the ADCP back and forth across the channel (**Figures S1-S4**). A total of 847 ADCP transects were acquired, of which 677 later passed rigorous quality-assurance screening and were used to compute 174 hourly in situ discharge measurements (**Figure S5, Tables S1-S2, Datasets S1-S3**).

Simultaneous measurements of ice surface motion were collected every 5 seconds using a Trimble R7 GPS receiver and Trimble Zephyr Geodetic antenna anchored in the ice (67.048°N, -49.018 °W, elevation 1211.43 m). On-ice kinematic GPS positions were later estimated using carrier-phase differential processing relative to a bedrock mounted base station (67.150°N, -50.058°W, elevation 581.19) and final International GNSS Service satellite orbits (*Chen, 1998; Estey & Meertens, 1999; Hoffman et al., 2011; Andrews al. 2014; 2018*; see SI). To assess surface melt processes, simultaneous measurements of 2-m air temperature, energy balance, and ice ablation were obtained using the nearby PROMICE KAN_M automated weather station (AWS) (*Fausto and van As, 2019*). To assess proglacial water outflow, hourly discharges were obtained from permanent river gauges at Qinnguata Kuussua (Watson River) in Kangerlussuaq (*van As et al., 2019*), and its northern tributary Akuliarusiarsuup Kuua near the ice terminus (*Rennermalm et al., 2017*, AK4 station 67.146°N, 50.107°W). Lagged correlation coefficients were used to quantify links among these various forcing variables with GPS-derived ice motion.

2.2 Proxies for *S* and Δ*S*

GPS-derived vertical positions and their first derivative were used to estimate subglacial storage *S* and rate-of-change Δ*S* (e.g. *Cowton et al., 2016; Bartholomew et al., 2012;* see **SI**). Proxies for *S* and Δ*S* were also computed by adapting a meltwater input-output approach (*Bartholomaus et al. 2008; 2011; McGrath et al. 2011*) comparing relative timings of supra- and proglacial discharge hydrographs (see **SI**). Hydrographs were normalized and differenced (supraglacial minus proglacial) to assess their relative timings and shapes at Rio Behar moulin and at the ice edge. These "discharge-difference" proxies are unitless and do not satisfy mass conservation so should be used qualitatively (i.e. for visual comparison of peak *S* and *ΔS* timing with accelerations in ice speed). They also characterize instantaneous net water storage, not subglacial routing delays and/or storages known to retard proglacial discharges longer than 24 h (e.g. *Chandler et al., 2013; Chu et al., 2016; Pitcher et al. 2020; Rennermalm et al., 2013b; Smith et al., 2015; van As et al., 2017*). Dye tracing experiments, for example, show that subglacial routing from ~1300 m elevation takes 1-3 days (*Chandler et al. 2013,* site L57), or ~2-5 days from proglacial hydrograph analysis (*van As et al., 2017*). Such subglacial delays and storages are irrelevant to our purpose here, which is simply to characterize instantaneous subglacial conditions at our field site, not Lagrangian transport to the ice edge. Complete description of these data and methods are presented in **SI**.

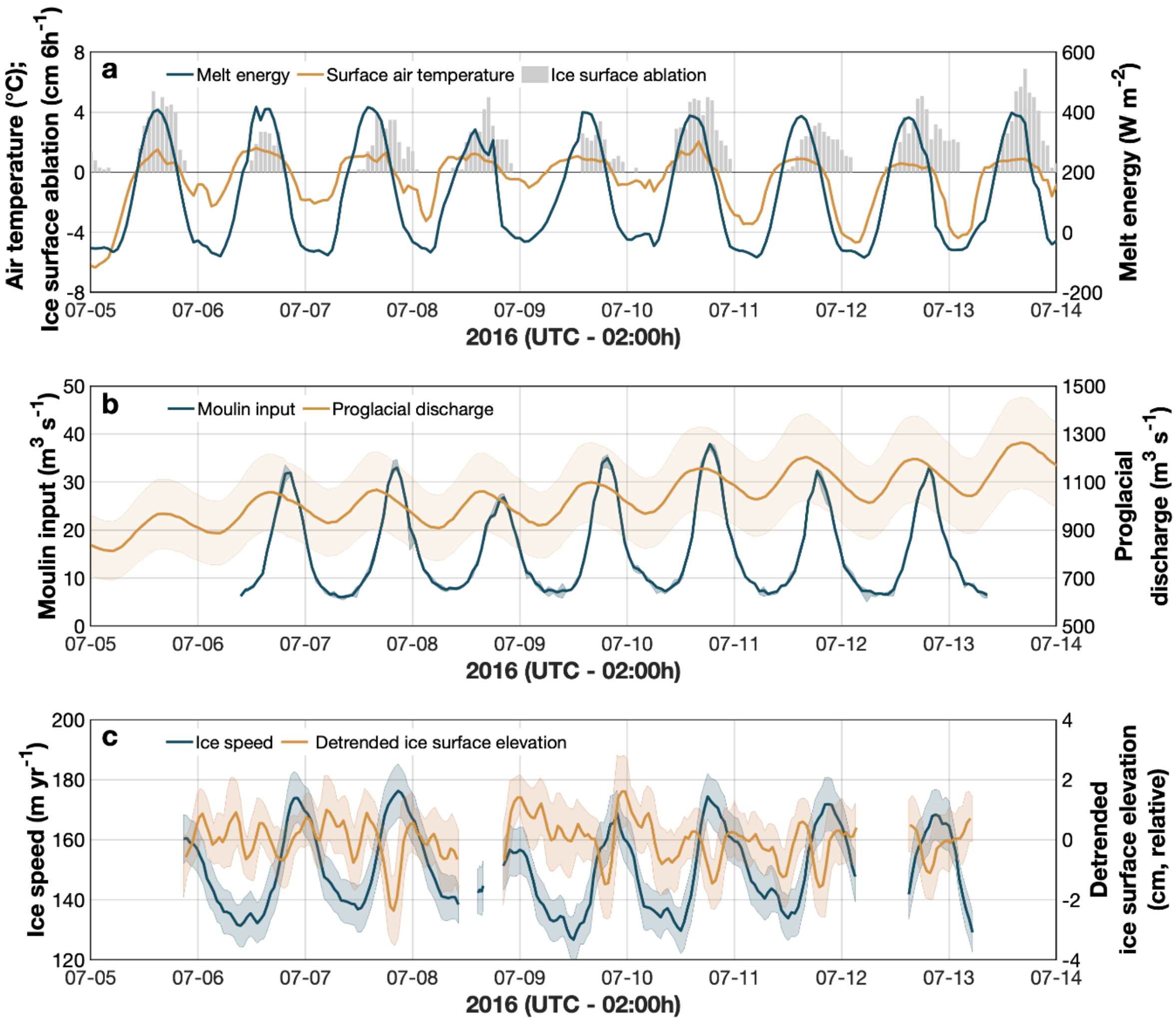

Figure 2: In situ measurements of (a) melt energy, air temperature, and ice ablation from PROMICE KAN_M; (b) Rio Behar moulin input (supraglacial river discharge) and proglacial discharge at Kangerlussuaq; (c) Rio Behar ice surface speed and elevation. Colored envelopes (b, c) represent measurement uncertainties of discharge and ice motion (see SI).

3. Results

3.1 Correlations of ice speed with other variables

We find strong diurnal cycles in all variables except surface elevation, with daily accelerations in horizontal ice speed closely tracking melt energy and moulin input (**Figure 2**). A consistent progression is observed in the timing of daily peaks, with melt energy and air temperatures peaking near local solar noon, followed by sequential peaks in ice ablation, moulin input, ice speed, and proglacial discharge (**Figure 3**). The timing of daily peaks is most consistent for melt energy, moulin input, ice velocity, and proglacial discharge, whereas peaks in

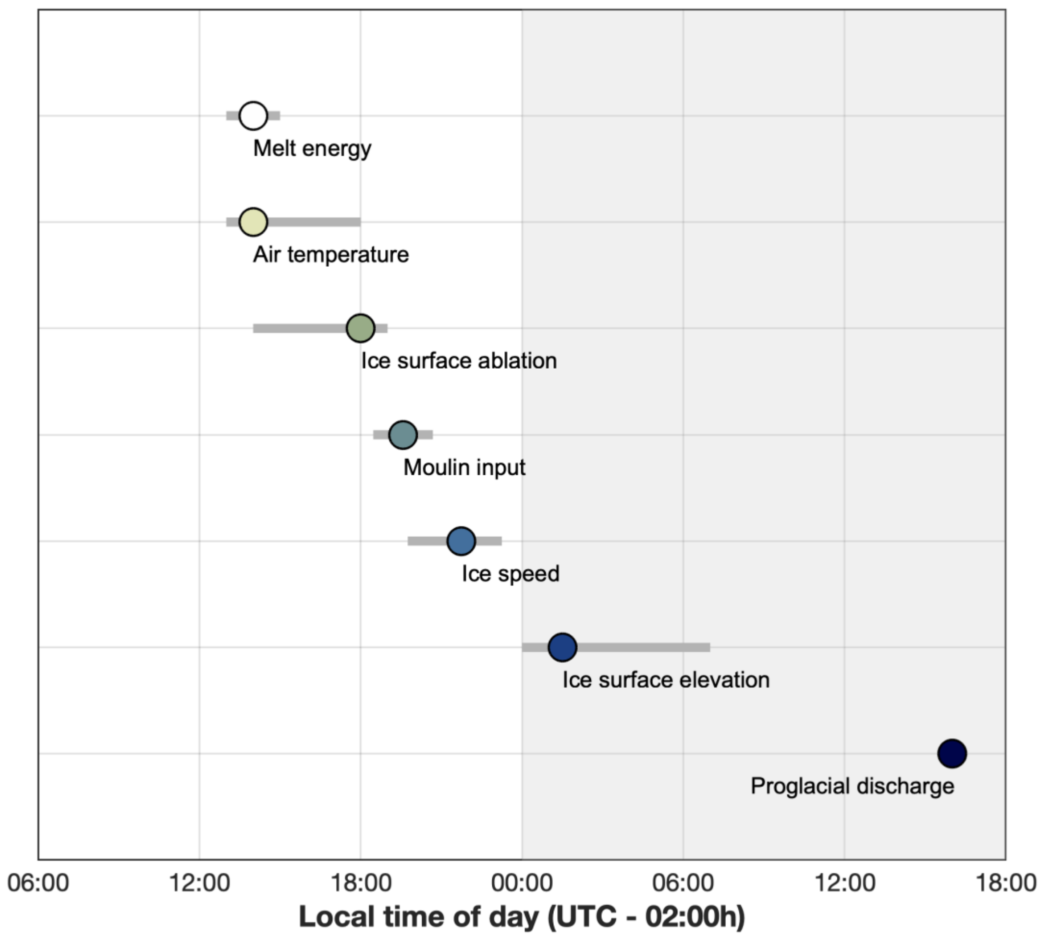

air temperature, ablation, and ice surface elevation are more temporally variable (**Figure 3**).

Figure 3: Mean daily timing (circles) and timing range (earliest to latest, grey bars) of daily peaks in observed variables. Diurnal cycles in melt energy and air temperatures peak around solar noon, followed by peaks in ice ablation, moulin meltwater input, ice surface speed, ice surface uplift, and proglacial discharge. Peak proglacial discharge displays no timing variability and is here shifted -8h to account for the mean timing difference between peak daily discharge observed at Kangerlussuaq versus at the ice edge (see SI). Note that this figure presents only the timing of daily peaks, not subglacial routing and/or storages known to delay proglacial discharges longer than 24h.

After lagging our GPS-derived horizontal ice speed time-series to correct for mean timing differences with the other variables, we find ice speed correlates most strongly with melt energy and moulin input (r=0.9, **Figures 4a, 4d**). Moderately strong correlations are found for air temperature (r=0.71, **Figure 4b**) and ice surface ablation rate (r=0.75, **Figure 4c**), drivers of melt energy and runoff, respectively. Lower correlations are found for detrended proglacial discharge (r=0.74, **Figure 2b**) and detrended ice surface elevation (i.e. uplift, r=0.37, **Figure 4e**). All correlations are statistically significant (p<0.01). Unlike melt energy (which turns negative, suggesting nocturnal refreezing), moulin input persists at low levels throughout the night. Because i) moulin input closely tracks (and derives from) melt energy; ii) virtually all meltwater runoff generated within Rio Behar catchment flows to its moulin; and iii) the observed +5h timing difference between peak melt energy and peak supraglacial discharge is similar to a previously calculated catchment routing delay for Rio Behar (i.e. estimated time-to-peak t_p=5.5h, *Smith et al., 2017*) we infer that supraglacial river discharge, a product of catchment-integrated

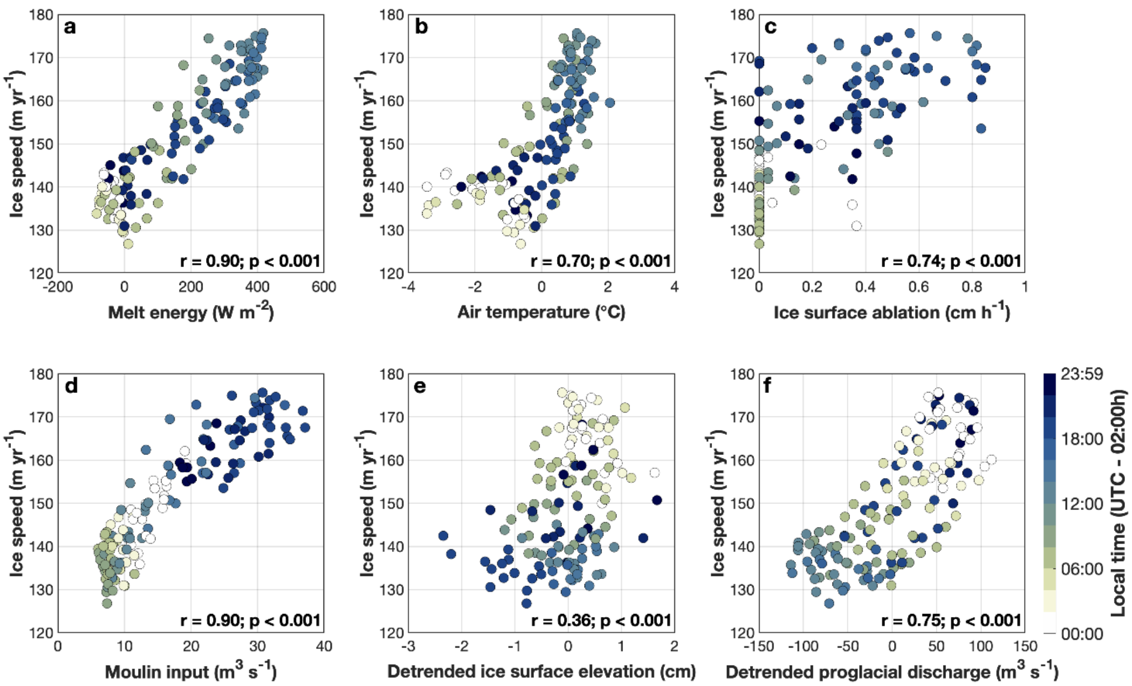

melt energy, is a dominant forcing variable driving our locally recorded ice-speed variations.

Figure 4. Correlations between ice speed and other observed variables, after correcting for the mean differences in daily peak timing shown in Figure 3 (timing differences in parentheses): (a) melt energy (-7h); (b) air temperature (-7h); (c) ablation (-4h); (d) moulin input (-2h); (e) ice surface elevation (+6h); (f) proglacial discharge (+19h at the ice sheet edge). Linear correlations (*r*) and statistical probability values (*p*) are shown in the bottom right corner of each plot. Strongest correlations with ice speed are found for melt energy and moulin input.

3.2 Comparison of short-term ice accelerations with *S* and Δ*S*

To further investigate drivers of ice speed variations, we test proxies of subglacial water storage *S* and rate-of-change Δ*S* calculated from GPS-derived ice surface observations (*Anderson et al., 2004; Andrews et al., 2018; Cowton et al., 2016; Harper et al., 2007; Hoffman et al., 2011; Howat et al., 2008*) and by differencing normalized hydrographs of supraglacial and proglacial river discharge (See **Methods** and **SI**). Implicit in the latter discharge-difference calculations are assumptions that englacial storage is negligible; that en/subglacial melting is negligible; that subglacial routing delays are irrelevant to instantaneous net storage; and that distal (>40 km) proglacial discharge reflects overall regional basal water pressure, allowing Rio Behar moulin input to be compared with regional proglacial discharge despite its smaller spatial domain (60 km^2 vs. ~2800 km^2 to 1750 m a.s.l.) and absolute discharge magnitude (~6-38 $m^3 s^{-1}$ vs. ~800-1300 $m^3 s^{-1}$).

Comparison of our observed horizontal ice speeds with both proxies for *S* and Δ*S* suggests that Δ*S* drives short-term accelerations in ice speed (**Figure 5b**). This conclusion is clearest from the discharge-difference proxies, with Δ*S* aligning better with ice speed peaks and ascents than *S* (see **Figure 5c** versus **Figure 5b**, see also **Figure S7)**. This same conclusion may be drawn, albeit less compellingly, from conventional GPS-derived *S* and Δ*S* proxies (i.e. **Figure 5a** versus **Figure 2c**; **Figure S7**). For both methods, peaks in Δ*S* generally align better with ice accelerations than peaks in *S*, suggesting that changes in subglacial water storage force short-term ice speed accelerations at our field site.

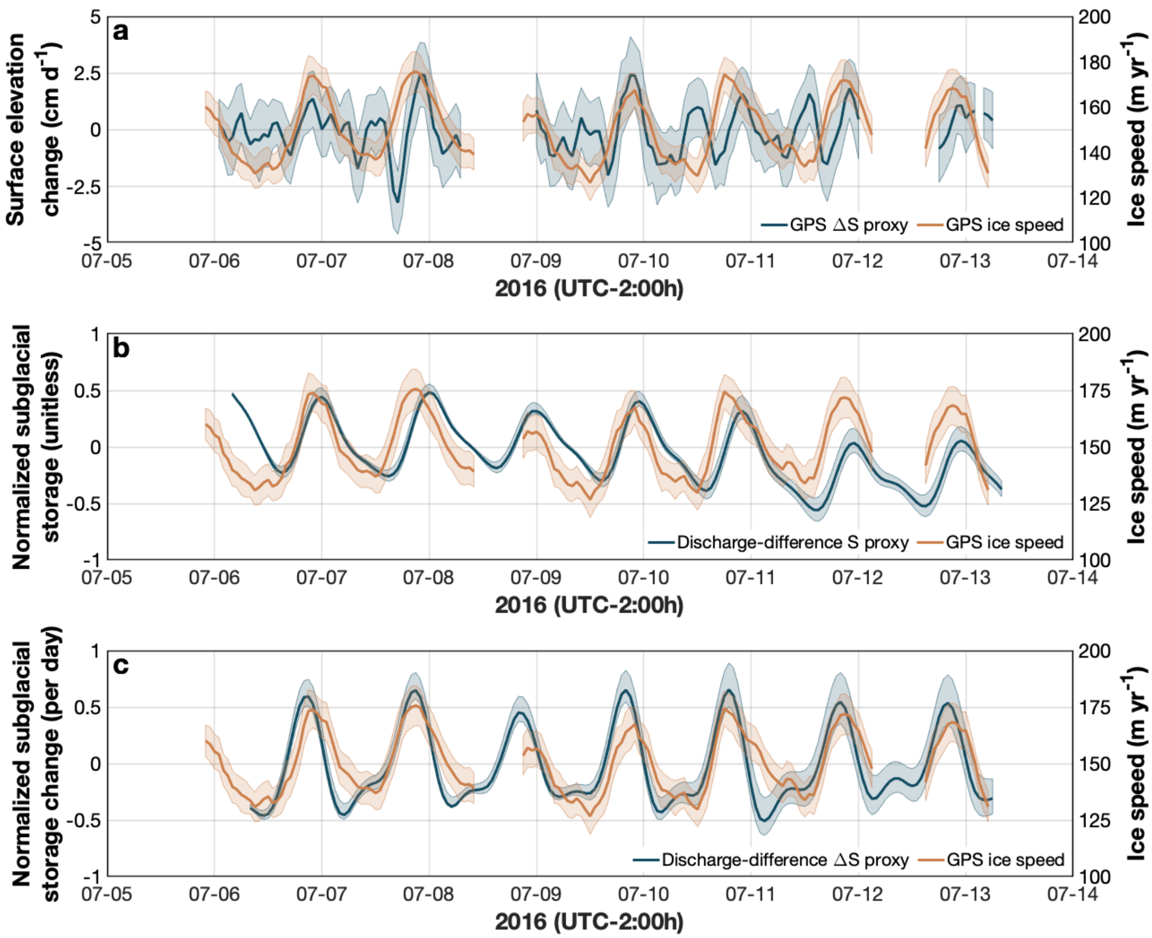

Figure 5. Comparison of horizontal ice speeds (blue line) with proxies for subglacial water storage (*S*) and its rate-of-change (Δ*S*): (a) Δ*S* as estimated from GPS-derived ice surface elevations; (b) *S* as estimated from normalized discharge-difference; (c) Δ*S* as estimated from normalized discharge-difference. See Figure 2(c) for *S* as estimated from GPS. Short-lived accelerations in ice speed generally align with peaks or ascents in *S* (c), see also (a); but not *S* (b), see also Figure 2(c). Peaks in Δ*S* capture peaks in ice speed more exclusively in (c) than (a),

and also some small secondary ice accelerations, suggesting that the discharge-difference proxy may more sensitively characterize subglacial water storage conditions than vertical GPS measurements.

4. Discussion and conclusion

We find that diurnal cycles in moulin input (following the integrative and delaying effects of surface routing through the upstream catchment) are the primary driver of short-term accelerations in ice sliding velocity (**Figure 3, Figure 4**). This finding supports previous work (*Andrews et al., 2014*) and the conclusion that over diurnal scales, supraglacial rivers impose a first-order control on subglacial water pressure fluctuations. Furthermore, while short-term accelerations in ice speed closely follow moulin input (**Figure 2, Figure 4**), they also tend to align with proxies for subglacial water storage change (ΔS) better than proxies for absolute storage (S) (**Figure 5, see also Figure 2c**), suggesting that nocturnal peaks in subglacial water storage drive subglacial basal pressure and short-term ice motion.

This conclusion is more evident in discharge-difference proxies (**Figures 5b, 5c**) than conventional GPS-derived proxies (**Figures 2c, 5a**). The discharge-discharge ΔS proxy reflects quiescent periods better than GPS-derived ΔS, and may also reflect subglacial behavior associated with a secondary ice-speed peak on most days (**Figure 5c**). Differencing supra- and proglacial hydrographs, therefore, may characterize subglacial water storage conditions more sensitively than small vertical ice surface elevation changes, which are inherently difficult to detect and have multiple sources of uncertainty (*Anderson et al., 2004; 2018*). A meltwater input-output approach (here adapted from *Bartholomaus et al., 2008; 2011* and *McGrath et al., 2011*), comparing moulin inputs with proglacial outputs, offers an alternate strategy for characterizing subglacial water storage and their link to ice and basal sliding laws. Future studies, for example, could develop discharge-difference proxies over longer time scales and larger study areas by pairing surface-routed climate model output (e.g. *Smith et al., 2017; Yang et al., 2019*) with proglacial discharge records (*Rennermalm et al. 2017; van As et al., 2019*), to relate net increases/decreases in ΔS to ice speed variations. Our results, using normalized input and output without mass conservation, suggest that a true (i.e. mass-conserved) water balance may not even be necessary to infer qualitative relationships between subglacial water storage, subglacial pressures, and ice motion.

It is well-known that evolution of the subglacial system from inefficient to efficient states acts to modulate the ice dynamical response to supraglacial inputs (e.g. *Bartholomew et al., 2010; 2011; Hoffman et al., 2011*). Using two different methods, we find that peak or ascendant ΔS is associated with localized GrIS velocity accelerations (**Figure 5c**). This suggests that highest subglacial water pressures (and ice sliding speeds) occur when subglacial cavities are growing the fastest, not when their size is largest (e.g. *Iken et al., 1983; Cowton et al., 2016*) As such, steady-state theoretical basal sliding laws – which assume a relationship between cavity size and subglacial pressure – do not accurately represent transient behavior of the subglacial system.

It is important to note that the strong correlation between moulin input and ice velocity reported here (**Figure 4d**) is unlikely to hold over an entire melt season. Previous work has clearly established that Greenland ice sliding velocities are strongly influenced by long-term seasonal evolution of the subglacial hydrological system (*Hoffman et al., 2011; Andrews et al., 2018; Bartholomew et al., 2010; Nienow et al., 2017*). Our short 7-day record captures neither the early nor late melt season, when subglacial efficiency (and associated ice speeds) undergo extensive changes. Subglacial evolution makes melt-driven proxies inappropriate for estimating ice motion over the entire melt season (*Andrews et al., 2014, Bartholomew et al., 2010*) or multiple years (*Tedstone et al., 2015; Davison et al., 2019*). Over short time scales, however, we find that diurnal cycles in moulin input are the primary driver of fluctuating subglacial water pressures and associated ice accelerations – even in relatively thick ice (~1 km) more than 40 km inland from the ice edge. Some slight variability in peak timings between Δ*S* and ice motion, as well as non-linear behavior on descending limbs (**Figure 5c**) are discussed further in **SI** (**Text S8**)

This study adds to a small but growing collection of GrIS supraglacial streamflow measurements (*Holmes 1955; Echelmeyer and Harrison 1990; Carver et al. 1994; McGrath et al. 2011; Chandler et al., 2013; Gleason et al. 2016; Smith et al., 2015; 2017*). With peak daily discharges of 26.59 – 37.61 m^3/s (**Table S2**), the discharges reported here are far larger than those collected in most supraglacial streams, but are typical for trunk supraglacial rivers in southwest Greenland (*Smith et al., 2015; 2017*). Nearly all of them terminate in moulins (*Smith et al., 2015; Yang and Smith, 2016*), and the high diurnal variability we observe (19.05 – 30.50 m^3/s, **Table S2**) signifies that local subglacial channels are likely out of equilibrium with moulin input for large portions of the day, such that corresponding accelerations in ice speed are driven by addition or removal of water outside of the channelized system.

Based on satellite mapping (e.g. *Yang and Smith, 2013; 2016; Lampkin and VanderBerg, 2014; Smith et al., 2015; Yang et al., 2015; 2016)* and topographic modeling (e.g. *Banwell et al. 2012; 2016; King et al., 2016; Karlstrom and Yang, 2016; Crozier et al., 2018*), we submit that supraglacial rivers likely drive ice accelerations near hundreds of other terminal moulins as well. Process-level understanding and modeling of subglacial hydrology and associated ice dynamics should presume large, strongly diurnal inputs of meltwater entering hundreds of supraglacial river moulins distributed throughout Greenland's ablation zone. These inputs, countered by water output discharged beneath outlet glaciers, trigger short-term fluctuations in subglacial water storage that drive short-term accelerations in ice sheet motion.

5. Data Availability

Supraglacial discharges, surface mass balance variables, ADCP and GPS data, and *S* and Δ*S* proxies are provided as summary tables (**Tables S1-S2**) and/or as Additional Supporting Information (**Datasets S1-S7**). PROMICE KAN_M automated weather station data (*Fausto and van As, 2019*) are available from https://www.promice.org/PromiceDataPortal/). Proglacial river discharges for Qinnguata Kuussua/Watson River (*van As et al., 2019*) and Akuliarusiarsuup Kuua (*Rennermalm et al., 2013b; 2017*) are available from https://doi.org/10.22008/promice/data/watson_river_discharge and https://doi.org/10.1594/PANGAEA.876357.

6. Acknowledgements

This research was funded by the NASA Cryospheric Science Program (grants 80NSSC19K0942 and NNX14AH93G) managed by Dr. Thorsten Markus. Polar Field Services, Inc. and Kangerlussuaq International Science Support (KISS) provided logistical field support. GPS equipment was loaned by UNAVCO, Inc. with support from NASA and NSF. A. Zaino and J. Pettit of UNAVCO advised on GPS receiver hardware, programming, and installation. Proglacial discharge data from Qinnguata Kuussua/Watson River were gathered by the University of Copenhagen and the Geological Survey of Denmark and Greenland. The KAN_M weather station is part of the Programme for Monitoring of the Greenland Ice Sheet (www.PROMICE.dk). The authors declare there are no real or perceived financial conflicts of interest, or other affiliations for any author that may be perceived as having a conflict of interest with respect to the results of this research.

Dedication

We dedicate this paper to the memory of Konrad Steffen (1952-2020).

References

Andrews L.C., Catania G.A., Hoffman M.J., Gulley J.D., Lüthi M.P., et al. (2014), Direct observations of evolving subglacial drainage beneath the Greenland Ice Sheet. *Nature*, 514, 80–83, https://doi.org/10.1038/nature13796

Andrews, L.C., Hoffman, M.J., Neumann, T.A., Catania, G.A., Lüthi, M.P., Hawley, R.L., et al. (2018), Seasonal evolution of the subglacial hydrologic system modified by supraglacial lake drainage in western Greenland. *Journal of Geophysical Research-Earth Surface*, 123, 1479–1496. https://doi.org/10.1029/

Anderson, R.S., Anderson, S.P., MacGregor, K.R., Waddington, E.D., O'Neel, S., Riihimaki, C.A., Loso, M.G. (2004), Strong feedbacks between hydrology and sliding of a small alpine glacier. *Journal of Geophysical Research—Earth Surface*, 109(F3), F03005. https://doi.org/10.1029/2004JF000120

Banwell, A.F., Arnold, N.S., Willis, I.C., Tedesco, M., Ahlstrom, A.P. (2012), Modelling supraglacial water routing and lake filling on the Greenland ice sheet. *J. Geophys. Res.*, 117, F04012, doi:10.1029/2012JF002393.

Banwell, A., Hewitt, I., Willis, I., Arnold, N. (2016), Moulin density controls drainage development beneath the Greenland ice sheet. *J. Geophys. Res. Earth Surf.*, 121, 2248–2269, doi:10.1002/2015JF003801.

Bartholomaus, T.C, Anderson, R.S., Anderson, S.P. (2008), Response of glacier basal motion to transient water storage. *Nature Geoscience*, 1, 33–37. https://doi.org/10.1038/ngeo.2007.52

Bartholomaus, T.C., Anderson, R.S., Anderson, S.P. (2011), Growth and collapse of the distributed subglacial hydrologic system of Kennicott Glacier, Alaska, USA, and its effects on basal motion. *Journal of Glaciology*, 57(206), 985-1002, DOI: https://doi.org/10.3189/002214311798843269

Bartholomew, I., Nienow, P., Mair, D. et al. (2010), Seasonal evolution of subglacial drainage and acceleration in a Greenland outlet glacier. *Nature Geosci*., 3, 408–411, https://doi.org/10.1038/ngeo863

Bartholomew, I., Nienow, P., Sole, A., Mair, D., Cowton, T., Palmer, S., Wadham, J. (2011), Supraglacial forcing of subglacial drainage in the ablation zone of the Greenland ice sheet. *Geophys. Res. Lett*., 38, L08502, doi:10.1029/2011GL047063.

Bartholomew, I. D., Nienow, P., Sole, A., Mair, D., Cowton, T., King, M. A. (2012), Short-term variability in Greenland Ice Sheet motion forced by time-varying meltwater drainage: Implications for the relationship between subglacial drainage system behavior and ice velocity. *Journal of Geophysical Research: Earth Surface, 117*(F3), F03002. https://doi.org/10.1029/2011JF002220

Bell, R. (2008) The role of subglacial water in ice-sheet mass balance. *Nature Geosci*, 1, 297–304, https://doi.org/10.1038/ngeo186

Bindschadler, R. (1983), The importance of pressurized subglacial water in separation and sliding at the glacier bed. *Journal of Glaciology*, 29(101), 3–19. https://doi.org/10.3189/S0022143000005104

Carver S., Sear D.,Valentine E. (1994) An observation offroll waves in a supraglacial meltwater channel, Harlech Gletscher, East Greenland. *J. Glaciology* 40(134):75–78

Catania G.A., Neumann T.A. (2010), Persistent englacial drainage features in the Greenland Ice Sheet. *Geophys. Res. Lett*, 37:1–5, https://doi.org/10.1029/2009GL041108

Chandler, D. M., Wadham, J. L., Lis, G. P., Cowton, T., Sole, A., Bartholomew, I., … Hubbard, A. (2013), Evolution of the subglacial drainage system beneath the Greenland Ice Sheet revealed by tracers. *Nature Geoscience*, 6(3), 195–198. https://doi.org/10.1038/ngeo1737

Chen, G. (1998). GPS kinematic positioning for airborne laser altimetry at Long Valley, California. Massachusetts Institute of Technology, Cambridge, MA. Retrieved from http://dspace.mit.edu/handle/1721.1/9680

Chu, V. W. (2014), Greenland ice sheet hydrology: a review, *Prog. Phys. Geogr*., 38(1), 19-54.

Chu W., Schroeder D.M., Seroussi H., Creyts T.T., Palmer S.J., Bell R.E. (2016), Extensive winter subglacial water storage beneath the Greenland Ice Sheet. *Geophys. Res. Lett.* 43(24):12,484-12,492

Clason C.C., Mair D.W.F., Nienow P.W., Bartholomew I.D., Sole A., et al. (2015), Modelling the transfer of supraglacial meltwater to the bed of Leverett Glacier, Southwest Greenland. *The Cryosphere*, 9(1), 123–38. www.the-cryosphere.net/9/123/2015/doi:10.5194/tc-9-123-2015

Cooper M.G., Smith L.C., Rennermalm A.K., Miège C., Pitcher L.H, et al. (2018), Meltwater storage in low-density near-surface bare ice in the Greenland ice sheet ablation zone. *The Cryosphere* 12(3):955–70

Cooper, M.G., Smith, L.C. (2019) Satellite Remote Sensing of the Greenland Ice Sheet Ablation Zone: A Review. *Remote Sensing*, 11, 2405. DOI: 10.3390/rs11202405

Cowton T., Nienow P., Sole A., Wadham J., Lis G., et al. (2013), Evolution of drainage system morphology at a land-terminating Greenlandic outlet glacier. *J. Geophys. Res. Earth Surf.* 118(1):29–41

Cowton, T., Nienow, P., Sole, A., Bartholomew, I., Mair, D. (2016), Variability in ice motion at a land-terminating Greenlandic outlet glacier: the role of channelized and distributed drainage systems. *Journal of Glaciology*, doi:10.1017/jog.2016.36

Crozier, J., Karlstrom, L., and Yang, K. (2018), Basal control of supraglacial meltwater catchments on the Greenland Ice Sheet, *The Cryosphere*, 12, 3383–3407, https://doi.org/10.5194/tc-12-3383-2018

Davison, B.J., Sole, A.J., Livingstone, S.J., Cowton, T.R., Nienow, P.W. (2019) The influence of hydrology on the dynamics of land-terminating sectors of the Greenland ice sheet. *Frontiers in Earth Science*, 7(10), ISSN 2296-6463 https://doi.org/10.3389/feart.2019.00010

Echelmeyer K., Harrison W.D. (1990) Jakobshavns Isbræ, West Greenland: seasonal variations in velocity—or lack thereof. *J. Glaciology*, 36(122):82–88.

Estey, L.H., and Meertens, C.M. (1999) TEQC: The Multi-Purpose Toolkit for GPS/GLONASS Data. GPS Solutions (pub. by John Wiley & Sons), Vol. 3(1), 42-49, https://doi.org/10.1007/PL00012778

Fausto, R.S. and van As, D., (2019). Programme for monitoring of the Greenland ice sheet (PROMICE): Automatic weather station data. Version: v03, Dataset published via Geological Survey of Denmark and Greenland. DOI: https://doi.org/10.22008/promice/data/aws

Flowers, G., Jarosch, A., Belliveau, P., Fuhrman, L. (2016), Short-term velocity variations and sliding sensitivity of a slowly surging glacier. *Annals of Glaciology*, 57(72), 71-83. doi:10.1017/aog.2016.7

Flowers, G.E. (2018), Hydrology and the future of the Greenland Ice Sheet. *Nature Communications*, 9(2729). DOI: 10.1038/s41467-018-05002-0

Gagliardini, O., Cohen, D., Råback, P. Zwinger, T. (2007) Finite-element modeling of subglacial cavities and related friction law. J. Geophys. Res. 112, F02027.

Gleason, C.J., Smith, L.C., Chu, V.W., Legleiter, C.J., Pitcher, L.H., Overstreet, B.T., Rennermalm, A.K., Forster, R.R., and Yang, K. (2016), Characterizing supraglacial meltwater channel hydraulics on the Greenland Ice Sheet from in situ observations. *Earth Surf. Process. Landforms*, 41: 2111– 2122. doi: 10.1002/esp.3977.

Harper, J. T., Humphrey, N. F., Pfeffer, W. T., Lazar, B. (2007), Two modes of accelerated glacier sliding related to water. *Geophysical Research Letters*, *34*(12), L12503. https://doi.org/10.1029/2007GL030233

Hoffman M.J., Catania G.A., Neumann T.A., Andrews L.C., Rumrill J.A. (2011), Links between acceleration, melting, and supraglacial lake drainage of the western Greenland Ice Sheet. *J. Geophys. Res.*, 116, F04035

Hoffman, M., Andrews, L., Price, S. et al. (2016), Greenland subglacial drainage evolution regulated by weakly connected regions of the bed. *Nature Communications*, 7, 13903. https://doi.org/10.1038/ncomms13903

Holmes G. 1955. Morphology and hydrology of the Mint Julep area, southwest Greenland. In Project Mint Julep: Investigation of Smooth Ice Areas of the Greenland Ice Cap, 1953; Part II: Special Scientific Reports. Maxwell Air Force Base, AL: Arct. Desert Tropic Inf. Cent., Res. Stud. Inst., Air Univ.

Howat, I.M., Tulaczyk, S., Waddington, E., Björnsson, H. (2008), Dynamic controls on glacier basal motion inferred from surface ice motion. *Journal of Geophysical Research: Earth Surface*, 113(F3), F03015. https://doi.org/10.1029/2007JF000925

Iken, A. Röthlisberger, H., Flotron, A., W. Haeberli, W. (1983) The uplift of Unteraargletscher at the beginning of the melt season — a consequence of water storage at the bed? J. Glaciol., 29(101), 28–47

Irvine-Fynn, T.D.L., A.J. Hodson, B.J. Moorman, G. Vatne, A.L. Hubbard (2011), Polythermal glacier hydrology: a review, *Rev. Geophys*., 49(4), RG4002.

Jansson, P. (1996), Dynamics and hydrology of a small polythermal valley glacier. *Geografiska Annaler: Series A, Physical Geography*, 78, 171–180.

Kamb, B. (1970), Sliding motion of glaciers: Theory and observation. *Reviews of Geophysics*, 8(4), 673–728. https://doi.org/10.1029/RG008i004p00673

Karlstrom, L., Yang, K. (2016), Fluvial supraglacial landscape evolution on the Greenland Ice Sheet, *Geophys. Res. Lett*., 43, 2683– 2692, doi:10.1002/2016GL067697.

King L., Hassan M.A., Yang K., Flowers G. (2016), Flow Routing for Delineating Supraglacial Meltwater Channel Networks. *Remote Sensing*, 8(12):988. doi:10.3390/rs8120988

Lampkin, D.J., VanderBerg, J. (2014), Supraglacial melt channel networks in the Jakobshavn Isbræ region during the 2007 melt season, *Hydrol. Process*., 28, 6038– 6053, doi: 10.1002/hyp.10085

Lindbäck, K., Pettersson, R., Hubbard, A.L., Doyle, S.H., van As, D., Mikkelsen, A.B., Fitzpatrick, A.A. (2015). Subglacial water drainage, storage, and piracy beneath the Greenland Ice Sheet. *Geophysical Research Letters*, 42(18), 7606–7614. https://doi.org/10.1002/2015GL065393

Mair, D., Sharp, M.J., Willis, I.C. (2002), Evidence for basal cavity opening from analysis of surface uplift during a high-velocity event: Haut Glacier d'Arolla, Switzerland. *Journal of Glaciology*, 48(161), 208–216. https://doi.org/10.3189/172756502781831502

McGrath D., Colgan W., Steffen K., Lauffenburger P., Balog J. (2011), Assessing the summer water budget of a moulin basin in the Sermeq Avannarleq ablation region, Greenland ice sheet. *J. Glaciol.* 57(205):954–64

Meierbachtol, T., J. Harper, N. Humphrey (2013), Basal Drainage System Response to Increasing Surface Melt on the Greenland Ice Sheet. *Science*, 341, 6147, 777-779. DOI: 10.1126/science.1235905

Morlighem, M., Williams, C. N., Rignot, E., An, L., Arndt, J. E., Bamber, J. L., … Zinglersen, K. B. (2017), BedMachine v3: Complete bed topography and ocean bathymetry mapping of Greenland from multibeam echo sounding combined with mass conservation, *Geophysical Research Letters*, 44, 11,051– 11,061. https://doi.org/10.1002/2017GL074954 [Data accessed 7/20 at Morlighem, M. et al. 2017, updated 2018. IceBridge BedMachine Greenland, Version 3. Boulder, Colorado USA. NASA National Snow and Ice Data Center Distributed Active Archive Center. doi: https://doi.org/10.5067/2CIX82HUV88Y]

Nienow, P.W., Sole, A.J., Slater, D.A., Cowton, T.R. (2017), Recent Advances in Our Understanding of the Role of Meltwater in the Greenland Ice Sheet System. *Curr Clim Change Rep* (2017) 3:330–344, DOI 10.1007/s40641-017-0083-9

Palmer S., Shepherd A., Nienow P., Joughin I. (2011), Seasonal speedup of the Greenland ice sheet linked to routing of surface water. *Earth Planet. Sci. Lett.* 302(3–4):423–28

Pitcher, L.H., Smith, L.C. (2019), Supraglacial Streams and Rivers. *Annual Review of Earth and Planetary Sciences*, 47(1), 421-452, https://doi.org/10.1146/annurev-earth-053018-060212

Pitcher, L.H., Smith, L.C., Gleason, C.J., Miege, C., Ryan, J.C., Hagedorn, B., van As, D., Chu, W., Forster, R.R. (2020) Direct observation of wintertime meltwater drainage from the Greenland Ice Sheet. *Geophysical Research Letters*, e2019GL086521, https://doi.org/10.1029/2019GL086521

Rennermalm, Å.K., Moustafa, S.E., Mioduszewski, J., Chu, V.W., Forster, R.R., Hagedorn, B., Harper, J.T., Mote, T.L., Robinson, D.A., Shuman, C.A., et al. (2013a), Understanding Greenland ice sheet hydrology using an integrated multi-scale approach. *Environ. Res. Lett*. 2013, 8, 015017.

Rennermalm, Å.K., Smith, L. C., Chue, V.W., Box, J.E., Forster, R.R., Van den Broeke, M. R. (2013b), Evidence of meltwater retention within the Greenland ice sheet. *The Cryosphere*, 7, 1433–1445, 2013. https://doi.org/10.5194/tc-7-1433-2013

Rennermalm, A.K., Smith, L.C., Hammann, A.C., Leidman, S.Z., Cooper, M.G., Cooley, S.W., Pitcher, L. (2017), River discharge at station AK-004-001, 2008 - 2016, version 3.0. The State University of New Jersey, *PANGAEA*, https://doi.org/10.1594/PANGAEA.876357

Ryan, J.C., Smith, L.C., van As, D., Cooley, S.W., Cooper, M.G., Pitcher, L.H, Hubbard, A. (2019), Greenland Ice Sheet surface melt amplified by snowline migration and bare ice exposure Science Advances 5(3), eaav3738, DOI: 10.1126/sciadv.aav3738

Schoof, C. (2010), Ice-sheet acceleration driven by melt supply variability. *Nature*. 468(7325):803

Schoof, C. (2005), The effect of cavitation on glacier sliding. *Proc. R. Soc. A.* 461609–627 http://doi.org/10.1098/rspa.2004.1350.

Schweizer, J., Iken, A. (1992), The role of bed separation and friction in sliding over an undeformable bed. *Journal of Glaciology*, 38(128), 77–92. https://doi.org/10.3189/S0022143000009618

Sugiyama, S., Gudmundsson, H. (2004), Short-term variations in glacier flow controlled by subglacial water pressure at Lauteraargletscher, Bernese Alps, Switzerland. *Journal of Glaciology*, 50(170), 353–362. https://doi.org/10.3189/172756504781829846

Shepherd, A., Hubbard, A., Nienow, P., King, M., McMillan, M., Joughin, I. (2009), Greenland ice sheet motion coupled with daily melting in late summer, *Geophys. Res. Lett*., 36, L01501, doi:10.1029/2008GL035758.

Smith, L.C., Chu, V.W., Yang, K., Gleason, C.J., Pitcher, L.H., Rennermalm, Å.K., et al. (2015), Efficient meltwater drainage through supraglacial streams and rivers on the southwest Greenland Ice Sheet. *Proceedings of the National Academy of Sciences*, 112 (4) 1001-1006. https://doi.org/10.1073/pnas.1413024112

Smith, L.C., Yang, K., Pitcher, L.H., Overstreet, B.T., Chu, V.W., Rennermalm, Å.K., et al. (2017), Direct measurements of meltwater runoff on the Greenland Ice Sheet surface. *Proceedings of the National Academy of Sciences*, 114(50), E10622-E10631, DOI: 10.1073/pnas.1707743114

Tedstone, A.J., Nienow, P.W., Sole, A.J., Mair, D.W.F., Cowton, T.R., Bartholomew, I.D., King, M.A. (2013) Greenland ice sheet motion insensitive to exceptional meltwater forcing. *Proceedings of the National Academy of Sciences*, 110 (49) 19719-19724; DOI: 10.1073/pnas.1315843110

Tedstone, A., Nienow, P., Gourmelen, N., Dehecq, A., Goldberg, D., Hanna, E. (2015), Decadal slowdown of a land-terminating sector of the Greenland Ice Sheet despite warming. *Nature*, 526, 692–695. https://doi.org/10.1038/nature15722

van As, D., Bech Mikkelsen, A., Holtegaard Nielsen, M., Box, J. E., Claesson Liljedahl, L., Lindbäck, K., Pitcher, L., Hasholt, B. (2017), Hypsometric amplification and routing moderation of Greenland ice sheet meltwater release. *The Cryosphere*, 11, 1371–1386, https://doi.org/10.5194/tc-11-1371-2017

van As, D., Bent Hasholt, Andreas P. Ahlstrøm, Jason E. Box, John Cappelen, William Colgan, Robert S. Fausto, Sebastian H. Mernild, Andreas Bech Mikkelsen, Brice P.Y. Noël, Dorthe Petersen, Michiel R. van den Broeke (2018) Reconstructing Greenland Ice Sheet meltwater discharge through the Watson River (1949–2017), Arctic, Antarctic, and Alpine Research, 50:1, DOI: 10.1080/15230430.2018.1433799

van As, D., Hasholt, B., Ahlstrøm, A.P., Box, J.E., Cappelen, J., Colgan, W., Fausto, R.S., Mernild, S.H., Mikkelsen, A.B., Noël, B.P.Y., Petersen, D., van den Broeke, M.R. (2018), Reconstructing Greenland Ice Sheet meltwater discharge through the Watson River (1949–2017), *Arctic, Antarctic, and Alpine Research*, 50:1, DOI: 10.1080/15230430.2018.1433799

van As, D., Hasholt, B., Ahlstrøm, A. P., Box, J. E., Cappelen, J., Colgan, W., Fausto, R.S., Mernild, S.H., Mikkelsen, A.P., Noël, B.P.Y., Petersen, D., van den Broeke, M. R. (2019). Programme for monitoring of the Greenland ice sheet (PROMICE): Watson river discharge. Version: v01, Dataset published via Geological Survey of Denmark and Greenland. https://doi.org/10.22008/promice/data/watson_river_discharge van de Wal, R. S. W., W. Boot, M. R. Van den Broeke, C. J. P. P. Smeets, C. H. Reijmer, J. J. A. Donker, J. Oerlemans (2008), Large and rapid melt-induced velocity changes in the ablation zone of the Greenland ice sheet, *Science*, 321(5885), 111-113.

van de Wal, R.S.W., Smeets, C.J.P.P., Boot, W., Stoffelen, M., van Kampen, R., Doyle, S.H., Wilhelms, F., van den Broeke, M.R., Reijmer, C.H., Oerlemans, J., Hubbard, A. (2015), Self-regulation of ice flow varies across the ablation area in south-west Greenland, *The Cryosphere*, 9, 603–611, https://doi.org/10.5194/tc-9-603-2015

Williams, J.J., Gourmelen, N., Nienow, P. (2020), Dynamic response of the Greenland ice sheet to recent cooling. *Sci Rep*, 10, 1647. https://doi.org/10.1038/s41598-020-58355-2

Yang, K., Smith, L.C., Supraglacial Streams on the Greenland Ice Sheet Delineated From Combined Spectral-Shape Information in High-Resolution Satellite Imagery. *IEEE Geoscience and Remote Sensing Letters*, 10(4), 801–805, doi:10.1109/LGRS.2012.2224316, 2013

K. Yang, Smith, L.C., Chu, V.W., Gleason, C.J., Li, M. (2015), A Caution on the Use of Surface Digital Elevation Models to Simulate Supraglacial Hydrology of the Greenland Ice Sheet. *IEEE Journal of Selected Topics in Applied Earth Observations and Remote Sensing*, 8(11), 5212-5224, doi: 10.1109/JSTARS.2015.2483483.

Yang K., Smith L.C. (2016), Internally drained catchments dominate supraglacial hydrology of the southwest Greenland Ice Sheet. J. *Geophys. Res. Earth Surf*., 1891–1910. doi:10.1002/2016JF003927

Yang, K., Smith, L.C., Karlstrom, L., Cooper, M.G., Tedesco, M., van As, D., Cheng, X., Chen, Z., Li, M.(2018), A new surface meltwater routing model for use on the Greenland Ice Sheet surface, *The Cryosphere*, 12, 3791–3811, https://doi.org/10.5194/tc-12-3791-2018

Yang, K., Smith, L.C., Fettweis, X, Gleason, C.J., Lu, Y., Li, M. (2019) Surface meltwater runoff on the Greenland ice sheet estimated from remotely sensed supraglacial lake infilling rate (2019). *Remote Sensing of Environment*, 234, 111459, https://doi.org/10.1016/j.rse.2019.111459

Yang, K., Sommers, A., Andrews, L.C., Smith, L. C., Lu, X., Fettweis, X., Li, M. (2020) Inter-comparison of surface meltwater routing models for the Greenland Ice Sheet and influence on subglacial effective pressures, *The Cryosphere Discuss*., https://doi.org/10.5194/tc-2019-255.

Zwally, H.J., Abdalati, W., Herring, T., Larson, K., Saba, J., Steffen, K. (2002), Surface melt induced acceleration of Greenland ice-sheet flow, *Science*, 297(5579), 218-222.